AFRL-AFOSR-UK-TR-2019-0042

Waveform Diversity and Frequency Sharing Techniques for Cognitive Radar Systems

Maria Greco
UNIVERSITY DI PISA
VIA GIROLAMO CARUSO 16
PISA, 56122
IT

08/14/2019
Final Report

DISTRIBUTION A: Distribution approved for public release.

Air Force Research Laboratory
Air Force Office of Scientific Research
European Office of Aerospace Research and Development
Unit 4515 Box 14, APO AE 09421

REPORT DOCUMENTATION PAGE

Form Approved
OMB No. 0704-0188

1. REPORT DATE *(DD-MM-YYYY)*
14-08-2019

2. REPORT TYPE
Final

3. DATES COVERED *(From - To)*
01 Apr 2013 to 31 Mar 2017

4. TITLE AND SUBTITLE
Waveform Diversity and Frequency Sharing Techniques for Cognitive Radar Systems

5a. CONTRACT NUMBER

5b. GRANT NUMBER
FA8655-13-1-3011

5c. PROGRAM ELEMENT NUMBER
61102F

6. AUTHOR(S)
Maria Greco

5d. PROJECT NUMBER

5e. TASK NUMBER

5f. WORK UNIT NUMBER

7. PERFORMING ORGANIZATION NAME(S) AND ADDRESS(ES)
UNIVERSITY DI PISA
VIA GIROLAMO CARUSO 16
PISA, 56122 IT

8. PERFORMING ORGANIZATION REPORT NUMBER

9. SPONSORING/MONITORING AGENCY NAME(S) AND ADDRESS(ES)
EOARD
Unit 4515
APO AE 09421-4515

10. SPONSOR/MONITOR'S ACRONYM(S)
AFRL/AFOSR IOE

11. SPONSOR/MONITOR'S REPORT NUMBER(S)
AFRL-AFOSR-UK-TR-2019-0042

12. DISTRIBUTION/AVAILABILITY STATEMENT
A DISTRIBUTION UNLIMITED: PB Public Release

13. SUPPLEMENTARY NOTES

14. ABSTRACT
Spectrum sensing and spectrum sharing are the two main functions that allow a cognitive radar to measure, sense, learn, and be aware of the parameters related to the radio channel characteristics. This research derives an algorithm for estimating the channel parameters that characterize the behavior of the primary users and a spectrum sharing method that exploits these estimates to minimize the interference between the radar and the primary user. The proposed method optimizes the performance of the radar and, at the same time, limits the interference received by the other users.

15. SUBJECT TERMS
EOARD, Cognitive Radar, Waveform Diversity

16. SECURITY CLASSIFICATION OF: a. REPORT	b. ABSTRACT	c. THIS PAGE	17. LIMITATION OF ABSTRACT	18. NUMBER OF PAGES	19a. NAME OF RESPONSIBLE PERSON
Unclassified	Unclassified	Unclassified	SAR		MILLER, KENT
					19b. TELEPHONE NUMBER *(Include area code)* 011-44-1895-616022

Standard Form 298 (Rev. 8/98)
Prescribed by ANSI Std. Z39.18

UNIVERSITÀ DI PISA

DIPARTIMENTO DI INGEGNERIA DELL'INFORMAZIONE

WAVEFORM DIVERSITY AND FREQUENCY SHARING TECHNIQUES FOR COGNITIVE RADAR SYSTEMS

Pietro Stinco, Maria S. Greco, Fulvio Gini

and

Braham Himed*

**collaborating engineer from the Air Force Research Laboratory*

Pisa, April 2017

This work has been funded by EOARD grant FA8655-13-1-3011 on "Waveform Diversity and Frequency Sharing Techniques for Cognitive Radar Systems".

Acknowledgement of Sponsorship: Effort sponsored by the Air Force Office of Scientific Research, Air Force Material Command, USAF, under grant number FA8655-13-1-3011. The U.S. Government is authorized to reproduce and distribute reprints for Government purpose notwithstanding any copyright notation thereon.

The authors certify that there were no subject inventions to declare during the performance of this grant.

CHAPTER 1

SPECTRUM SENSING AND SHARING

FOR COGNITIVE RADAR SYSTEMS

ABSTRACT

This chapter deals with the problem of Spectrum Sensing and Spectrum Sharing for Cognitive Radar operating in spectrally dense environments. Spectrum sensing and spectrum sharing are the two main functions that allow a cognitive radar to measure, sense, learn, and be aware of the parameters related to the radio channel characteristics. This paper focuses on the role of Compressed Sensing (CS) in Spectrum Sensing and on the problem of channel parameter estimation for Spectrum Sharing. This paper shows how CS can allow a significant reduction in acquisition time reducing the cost for high-resolution analog-to-digital converters with large dynamic range, and high speed signal processors. We derive an algorithm for estimating the channel parameters that characterize the behaviour of the primary users and a spectrum sharing method that exploits these estimates to minimize the interference between the radar and the primary user. The proposed method optimizes the performance of the radar and, at the same time, limits the interference received by the other users.

1. Introduction

Radar technology has been evolving towards higher resolution, high-precision detection instruments with an ever-increasing list of functionalities. One of the areas that have very good potential of combining the benefits of these developments is multifunctional radar systems. These systems join inside the same system, and simultaneously, multiple functions such as surveillance, tracking, confirmation of false alarm, back-scanning, clutter and interference estimation, which are traditionally performed by dedicated individual radars [1]-[2].

For these reasons, multifunctional radar systems should be able to work with wider frequency bands than traditional radar systems. Clearly, this is in contrast with the growth of activities in the area of civil communications, the emergence of new technologies and new services that involve a strong demand for spectrum allocation inducing a very strong pressure upon the frequency channels currently allocated to radars.

Some portions of the radar bands have been recently allocated to communication services. For instance, the International Telecommunication Union (ITU) decided to allocate the spectrum between 5150 and 5350 MHz and between 5470 and 5725 MHz on a co-primary basis to wireless access systems including RLANs (Radio Local Area Networks) [3]-[4]. In the United States, the National Telecommunications and Information Administration (NTIA) has recently devoted efforts on identifying frequency bands that could be made available for wireless broadband service provisioning. A total of 115 MHz of additional spectrum (1695-1710 MHz and 3550-3650 MHz bands) has been identified for wireless broadband implementation [5].

A recent work [6] focused on the primary-secondary sharing between a radar system and indoor system providing broadband services, considering an Air Traffic Control (ATC) radar operating in the 2.7-2.9 GHz band and a Surveillance Radar in the 16.7-17.3 GHz. The case study analysed in this work is an L-band radar that shares the same frequency band with a JTDIS (Joint Tactical Information Distribution System) radio system, supposed to be the primary user of the channel. The JTIDS is a radio system for exchanging tactical information between aircraft and ground stations or ships and between aircraft. The JTDIS radio system operates in the frequency band 969-1206 MHz, subdivided into sub-channels used for frequency hopping.

From the above examples, it is clear that the availability of frequency spectrum for multifunction radar systems has been severely compromised and the available frequency bands are continuously diminished.

This unique issue of spectrum crowding and steadily increasing radar requirements cannot be addressed by traditional modes of operation. Future systems require the ability to anticipate the behaviour of radiators in the operational environment. This in turn leads to the need for critical and new methodologies based upon cognition as an enabling technology [7]-[12].

The cognitive methodology to reduce mutual interference between the radar and the other radiating elements is based on two main concepts: Spectrum Sensing and Spectrum Sharing. Spectrum Sensing has the goal to recognize the frequencies used by other systems using the same spectrum in real time, while Spectrum Sharing has the goal to limit interference from the radar to other services and vice-versa.

Through these functions, a cognitive radar can obtain necessary observations about the radio frequency channel, such as the presence of other users and the appearance of spectrum opportunities, i.e. spectrum holes where it is possible to transmit without interfering with other users of the channel. After using this information, a cognitive radar is able to adapt its transmit and receive parameters, such as the transmission power and the operating frequency, in order to achieve efficient spectrum utilization.

In cognitive radio terminology, primary users is defined as the users who have higher priority or legacy rights on the usage of a specific part of the spectrum. On the other hand, secondary users, which have lower priority, exploit this spectrum in such a way that they do not cause interference to primary users.

Therefore, secondary users need to have cognitive radio capabilities, such as sensing the spectrum reliably to check whether a primary user is using it and to change the radio parameters to exploit the unused part of the spectrum.

In this work, we analyse the problem of a wideband radar system that shares the same frequency band with a communication system, the frequency band of the communication system is divided into several frequency channels used for dynamic spectrum access. The radar system is the secondary user while the communication system is the primary user of the channel.

As an illustrative example, Figure 1 shows the spectrum opportunities in the frequency channels. As apparent, the available spectrum is divided into narrow chunks of bands. Spectrum opportunity in this dimension means that not all the bands are used simultaneously at the same time; therefore, some bands might be available for opportunistic usage. To this end, a cognitive radar should detect the spectrum opportunities, selecting the best frequency channels and vacating the frequency when a primary user appears.

In this paper, we focus on two important topics, the use of CS for Spectrum Sensing and the problem of channel parameter estimation for Spectrum Sharing application. In particular, we analyse the use of CS, focusing on how this emerging technology can represent a helpful tool to solve some important problems related to the hardware requirement for the design of a responsive spectrum sensing system, which is able to react to the changes of the operating frequency channel quickly. As a matter of fact, to have high spectrum efficiency and high sensing accuracy, a cognitive radar has to perform real-time wideband monitoring of the licensed spectrum, using a dual-radio architecture [13]-[14], where one chain is dedicated to radar operations while the other chain is dedicated to spectrum sensing. The drawback of such approach is the hardware cost, as the related systems requires high sampling rate and high resolution Analog-to-Digital Converters (ADCs) with large dynamic range, plus the use of high speed signal processors. Moreover, when the required time used to estimate the spectrum occupancy is very short and the monitored frequency band is wide, the current generation ADCs are even unable to collect the required samples at the Nyquist-rate. A signal processing technique that can solve this problem is based on the use of Compressed Sensing.

Recent results on CS state that it is possible to reconstruct a sparse signal from random projections of the sensor data (see e.g. [15]-[17]). The number of random projections can be very small, in proportion to the number of the channels occupied by the other users. Under the hypothesis that the frequency spectrum of the other users is sparse, CS can be profitably used to solve the hardware constraints by reducing the sampling rate and decreasing the computational complexity.

The second problem considered in this paper is the estimation of the channel parameters that describe the behaviour of the primary users of the channels and how to exploit these estimates to minimize the interference between the radar and the communication system.

Analysing the behaviour of the primary users and exploiting the time history of the channel occupancy, the cognitive radar system can evaluate the probability to have a spectrum opportunity, i.e. the probability that the monitored frequency channel is free at the time of transmitting. Evaluating this probability, a cognitive radar can decide whether it is possible or not to transmit in the monitored frequency channel at the beginning of each time slot.

The remaining part of the paper is organized as follows. Section 2 introduces the channel models for frequency spectrum occupancy of the primary user, introducing the concept of interfering temperature and defining two models for the primary user dynamics and for the spectrum occupancy. Section 3 describes how CS-based techniques can be used for Spectrum Sensing. Section 4 describes how to estimate the main channel parameters and how to evaluate the probability to have a spectrum opportunity using these parameter estimates. Simulation results are reported both in Section 3 and in Section 4. Conclusions and final remarks are summarized in Section 5.

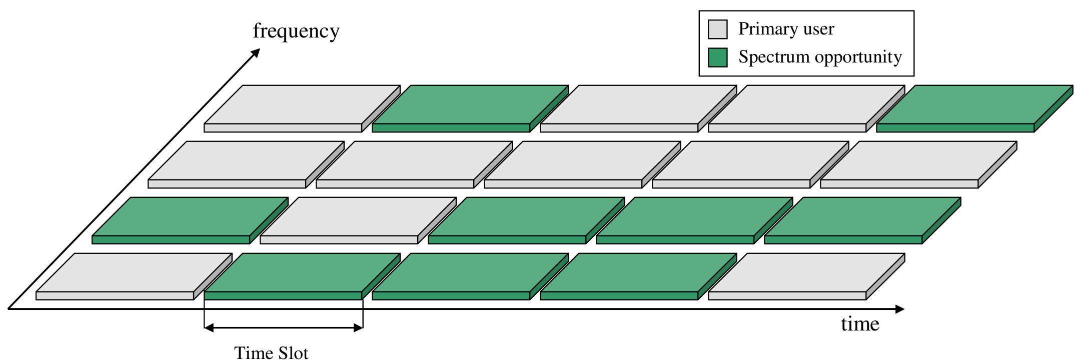

Figure 1 – Spectrum Opportunities.

2. Channel Model

As described, the cognitive radar is assumed to be the secondary user of the channel, therefore, it can use the spectrum only when it causes no harmful interference to the primary user. This requires a cognitive radar to be equipped with a spectrum sensing function, which can detect primary users' appearance and decide which portion of the spectrum is available.

Such a decision can be made according to various metrics. The traditional approach is to limit the transmitter power of interfering devices, i.e. the transmitted power should be no more than a prescribed noise floor at a certain distance from the transmitter.

However, due to the increased mobility and variability of radio frequency emitters, constraining the transmitter power becomes problematic, since unpredictable new sources of interference may appear. To address this issue, the FCC Spectrum Policy Task Force [18] has proposed a new metric on interference assessment, the interfering temperature, to enforce an interference limit perceived by receivers.

Like other representations of radio signals, instantaneous values of interference temperature would vary with time and, thus, would need to be treated statistically. In this section, we present a model for the interference temperature dynamics and the Hidden Markov Model (HMM) for channel occupancy.

2.1 *Interfering Temperature*

The FCC has proposed the interference temperature as a metric for interference analysis. The US Federal Communications Commission in 2002 investigated the future needs of radio frequency spectrum and the limitations of current spectrum policies, as well as develops recommendations for enhancing current policies. One recommendation was the use of an interference metric to enforce current spectrum access rights and create new opportunities for dynamic spectrum utilization [19]-[20]

The interference temperature is defined as the temperature equivalent of the RF power available at a receiving antenna per unit bandwidth [21], i.e.

$$T_I(f_C, B) = \frac{P_I(f_C, B)}{kB}, \quad (1)$$

where $P_I(f_C,B)$ is the average interference power in Watts, centered at f_C, covering bandwidth B measured in hertz, and Boltzmann's constant k is 1.38×10^{-23} JK^{-1}.

The FCC further established an interference temperature limit, which provides a maximum amount of tolerable interference for a given frequency band at a particular location. Any secondary transmitter using this band must guarantee that its transmission plus the existing noise and interference will not exceed the interference temperature limit at a primary user. Since any transmission in the licensed band is viewed to be harmful if it would increase the noise floor above the interference temperature limit, it is necessary that a cognitive radar receiver has a reliable spectral estimate of the interference temperature. Given a particular frequency band in which the interference temperature limit is not exceeded, that band could be made available for secondary usage. If a regulatory body sets an interference temperature limit T_L for a particular frequency band with bandwidth B, then the secondary user has to keep the average interference below kBT_L. Therefore, assuming that a secondary user is operating with average power P in a band $[f_C-B/2, f_C+B/2]$, the interference temperature limit will ensure that [21]:

$$T_I(f_C, B) + \frac{LP}{kB} \le T_L(f_C) \quad (2)$$

where L represents path loss attenuation between the secondary transmitter and the primary receiver.

2.2 *Statistical model for primary user's channel occupancy*

In this section, we introduce a statistical model for primary user's channel occupancy, describing the statistical model used to characterize the signal received by the cognitive radar and the statistical model for the observations at the output of the spectrum sensing detector.

The spectrum sensing module of the cognitive radar receiver periodically scans and senses multiple licensed channels to measure in each channel the interference temperature exploiting the received signal, then it compares the measured interference temperature with a predefined threshold value to evaluate if the channel is busy or free. However, due to the noise in the channel, a free channel can be classified as busy and a busy channel classified as free. In order to model the channel dynamics of the primary users, HMMs are proposed in [22]-[24]. In the context of dynamic spectrum access networks, HMMs are used to model the primary user occupancy of the channel. HMMs represent a useful tool for this problem since true occupancy states are not always known to the cognitive radar after the Spectrum Sensing process.

As discussed, the case study analysed in this work is related to an L-band surveillance radar, which shares the same frequency band with a JTDIS communication system. The frequency band used by the communication system is subdivided into N frequency channels of bandwidth B used for frequency division multiple access. As showed in Figure 1, the time axis is divided into time slots of duration Δt.

In general, a HMM is comprised of a set S_t of possible states and a set O_t of possible emissions. The possible states represent the real activity of the primary user in each frequency channel, if the primary user is transmitting at time slot t, the state is S_t=1, otherwise, if the channel is free, the state is S_t=0. However, due to the noise in the channel, a free channel can be classified as busy and a busy channel classified as free. Therefore, there are also two possible emissions, which are represented by the observation symbol O_t at the output of the spectrum sensing detector.

Figure 2 shows the HMM for spectrum occupancy in each frequency channel, in particular the lower part of the figure describes the primary user's dynamic while the upper part the secondary user's observation.

The primary user's dynamic is described by the states S_t=0 and S_t=1, and is characterized by the 2×2 state transition probability matrix **A**, that represents the probabilities associated with changing from one state to another and it is given by

$$[\mathbf{A}]_{hk} = a_{hk} = \Pr\left[S_t = h \mid S_{t-1} = k\right], \quad h,k=0,1. \tag{3}$$

In each frequency channel and in each time slot, if the primary user is transmitting, the received signal at the radar receiver is given by an oscillation at that frequency whose amplitude is a Gaussian random variable (r.v.) with zero mean and variance $\sigma_{\mathbf{f}}^2$, that is

$$\left[\mathbf{f}_i\right]_n = \alpha\zeta_i \cos\left(\frac{\pi(i-1)(2n-1)}{2N}\right), \quad i,n=1,\ldots,N, \tag{4}$$

where i is the frequency channel index, while n is the n-th time sample.

If the channel is free, the received signal $[\mathbf{f}_i]_n$ is zero. In each time slot, the multiband received signal is given by the combination of the signal in each frequency channel and Additive White Gaussian Noise (AWGN) with zero mean and variance $\sigma_{\mathbf{w}}^2$:

$$\mathbf{f} = \sum_{i=1}^{N} \mathbf{f}_i + \mathbf{w}\,. \tag{5}$$

The values of **A** may be different in each frequency channel.

The spectrum occupancy is given by the Discrete Cosine Transform (DCT) of **f**, that is

$$\mathbf{x} = \mathbf{\Psi}^T \mathbf{f}\,, \tag{6}$$

where $\mathbf{\Psi}$ is the DCT matrix whose elements are given by

$$\left[\mathbf{\Psi}\right]_{i,j} = \zeta_i \cos\left(\frac{\pi(i-1)(2j-1)}{2N}\right), \quad i,j=1,\ldots,N. \tag{7}$$

In (4) and (7) the values of ζ_i are given by

$$\zeta_i = \begin{cases} 1/\sqrt{N}, & i = 1 \\ \sqrt{2/N}, & 2 \le i \le N \end{cases} \tag{8}$$

Note that, in this work, without any lack of generality, we can consider real signals, instead of the complete complex signals. In fact, to monitor the spectrum occupancy of the primary users and to reduce the cost of the receiver further, it is not necessary to process the In-Phase (I) and Quadrature (Q) components of the received signal, but only one of them. Figure 3 shows the squared absolute value of $\mathbf{x}$, that is the channel occupancy evolution during an observation time composed of ten time slots Δt. The channel is composed of N=256 frequency bands and the Signal to Noise Ratio, defined as SNR= $\sigma_{\mathbf{f}}^2 / \sigma_{\mathbf{w}}^2$, is 20dB.

To evaluate the channel occupancy evolution it is necessary to perform the DCT of the received time samples every Δt seconds. When the frequency band to be monitored tends to be very wide and/or the time slot Δt tends to be very short, it should be very difficult to collect the N time samples at the Nyquist-rate. In Section 3, we study how CS may be used to alleviate this hardware constraint.

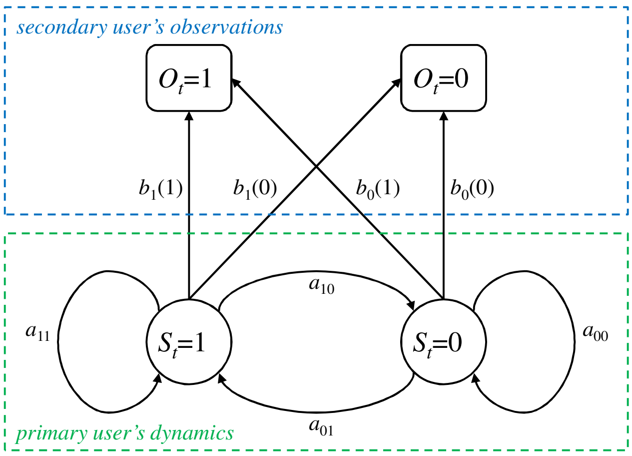

Figure 2 – Hidden Markov Model representation for spectrum occupancy.

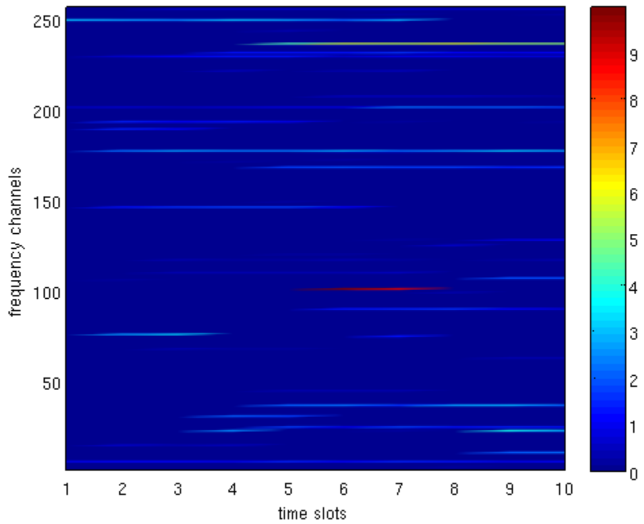

Figure 3 - Channel occupancy evolution in ten time slots, N=256, SNR=20dB.

In the open literature, there are several Spectrum Sensing techniques to recognize if the channel is occupied by the primary user, such as the energy detector, feature detector or matched filtering detection techniques [25]. In particular, at each time slot, the cognitive radar records an observation symbol O_t depending upon the following conditions:

$$\begin{cases} O_t = 0, & \text{if } T_I(t) \le T_L \\ O_t = 1, & \text{if } T_I(t) > T_L \end{cases} \tag{9}$$

The radar periodically makes the observations and records an observation sequence $\boldsymbol{O}=[O_1 \ldots O_T]$ over a period of T time slots. The transitions from the states S_t to the observations O_t are described by the 2×2 emission probability matrix **B**, which represents the probabilities associated with obtaining a certain output given that the model is currently in a true state s_t:

$$[\mathbf{B}]_{hk} = b_h(k) = \Pr\left[O_n = h \,|\, S_n = k\right]. \tag{10}$$

The emission probability matrix **B** is related to the Receiver Operating Characteristic (ROC) of the Spectrum Sensing detector. As a matter of fact, $b_0(1)$ is the probability of false alarm, that is the probability to classify a free channel as busy, whereas $b_1(0)$ is the probability of miss detection, that is the probability to classify a busy channel as free. Clearly, $b_0(0)=1-b_0(1)$ and $b_1(1)=1-b_1(0)$. These probabilities depend on the channel noise, the kind of signal emitted by the primary user and the spectrum sensing detector used at the cognitive radar receiver, that is on the specific characteristics of the systems that share the same channel. Knowing these characteristics, the elements of **B** can be calculated or evaluated through Monte Carlo simulations. Hence, without loss of generality, hereafter we assume that **B** is known. Section 4 will describe how to estimate the channel parameters from the observation sequence $\boldsymbol{O}$ and how to exploit these estimates to minimize the interference between the radar and the communication system.

3. Compressed Spectrum Sensing

In this section, after a brief introduction to the principles of Compressed Sensing (CS), we focus on its application to Spectrum Sensing, that will be referred to as Compressed Spectrum Sensing (CSS). For more details on CS we refer the reader to [15]-[17] and references therein.

CS is a signal processing methodology for signal recovery from highly incomplete information.

The central results state that a sparse vector[1] $\mathbf{x}\in\mathbb{R}^N$ can be recovered from a small number of linear measurements $\mathbf{y}=\mathbf{H}\mathbf{x}\in\mathbb{R}^K$, $K\ll N$ (or $\mathbf{y}=\mathbf{H}\mathbf{x}+\mathbf{w}$ when there is measurement noise) by solving a convex program [15]-[17]. To make this possible, CS relies on two principles: sparsity, which pertains to the signal of interest, and incoherence, which pertains to the sensing modality. Considering the real signal $\mathbf{f}\in\mathbb{R}^N$ defined in (5) and being $\mathbf{\Psi}=[\psi_1\ldots\ \psi_N]$ an orthonormal basis (e.g. the DCT), then the representation of **f** on the basis $\mathbf{\Psi}$ is given by $\mathbf{f}=\mathbf{\Psi}\mathbf{x}$, where **x** is the sparse coefficient vector. Given a set of vectors $[\varphi_1,\ldots,\varphi_K]$ and denoting with $\mathbf{\Phi}$ the $K\times N$ sensing matrix whose rows are the φ_k's, the measures are collected by means of

[1] A vector is s-sparse if it has at most s nonzero entries.

linear functionals $\mathbf{y}=\mathbf{\Phi f}=\mathbf{\Phi\Psi x}\in\mathbb{R}^K$ [15]-[16]. The interest is in undersampled situations in which the number K of available measurements is much smaller than the dimension N of the signal $\mathbf{f}$. The process of recovering the Kx1 vector $\mathbf{x}=\mathbf{\Psi}^T\mathbf{f}$ from the $N\times1$ measurement vector $\mathbf{y}=\mathbf{\Phi f}$ is, in general, ill-posed when $K<N$. However, if $\mathbf{x}$ is s-sparse, then the problem can be solved provided $K\geq s$. A necessary and sufficient condition for this problem is that, for some small $\delta>0$, the matrix $\mathbf{H}=\mathbf{\Phi\Psi}$ satisfies the Restricted Isometry Property (RIP) [26]:

$$(1-\delta)\|\mathbf{x}\|_2 \leq \|\mathbf{Hx}\|_2 \leq (1+\delta)\|\mathbf{x}\|_2 . \tag{11}$$

The RIP implies that matrix $\mathbf{H}$ must preserve the length of s-sparse vectors. A related condition to RIP is referred as *incoherence*. The coherence between the measurement matrix $\mathbf{\Phi}$ and the representation matrix $\mathbf{\Psi}$ measures the largest correlation between any two columns of these matrix and is defined as

$$\mu(\mathbf{\Phi},\mathbf{\Psi})=\sqrt{N}\max_{1\leq k,j\leq N}\left|\left\langle \varphi_k,\psi_j\right\rangle\right| . \tag{12}$$

It can be shown [15]-[17] that $\mu(\mathbf{\Phi},\mathbf{\Psi})\in\left[1,\sqrt{N}\right]$. The design of a measurement matrix $\mathbf{\Phi}$ such that $\mathbf{H}=\mathbf{\Phi\Psi}$ has the RIP requires that all possible combination of s nonzero entries on the vector $\mathbf{x}$ of length N have to satisfy (11). However, both the RIP and incoherence can be achieved with high probability by designing $\mathbf{\Phi}$ as a random matrix [15].

Now, it is natural to attempt to recover $\mathbf{x}$ by solving the following optimization problem:

$$\hat{\mathbf{x}}=\arg\min_{\mathbf{x}\in\mathbb{R}^N}\|\mathbf{x}\|_0,\ \text{s.t. } \mathbf{\Phi\Psi x}=\mathbf{y}. \tag{13}$$

In the literature, this minimization is referred as the Basis Pursuit (BP) method, which, for real valued signals, can be recast as a linear programming problem. The

BP method is guaranteed to find a reconstruction of a s-sparse signal if there is no measurement noise. However, in the presence of measurement noise, its influence on the signal reconstruction can be minimized by applying the Basis Pursuit De-Noising (BPDN) method which finds a solution of the following problem [27]:

$$\hat{\mathbf{x}} = \arg\min_{\mathbf{x}\in\mathbb{R}^N} \|\mathbf{x}\|_1, \text{ s.t. } \|\mathbf{y} - \mathbf{\Phi\Psi x}\|_2 \le \sigma, \tag{14}$$

where the positive parameter σ is an estimate of the noise level in the data. The case σ=0 corresponds to the basis pursuit problem. The BPDN method can be solved by means of linear programming algorithms.

As previously discussed, when the frequency spectrum of the user radiating in the same channel as the cognitive radar is a sparse signal, it is possible to apply CS ideas to Spectrum Sensing. For the problem at hand, the representation matrix $\mathbf{\Psi}$ is the DCT, whose elements are defined in (7). In this work, we consider two kind of measurement matrices $\mathbf{\Phi}$, the first one is the Gaussian matrix, which is formed by sampling independent and identically distributed (IID) entries from the normal distribution with zero mean and variance $1/K$:

$$[\mathbf{\Phi}]_{i,j} \sim N(0,1/K), \; i=1\ldots,K; j=1,\ldots,N. \tag{15}$$

The second measurement matrix is the Spiky matrix given by randomly selecting K rows of the $N\times N$ identity matrix. The latter case is the more interesting because, from the definition of this matrix, the measurement vector $\mathbf{y}$ is obtained by simply selecting K samples of $\mathbf{f}$ at random. The use of CS allows to use an ADC with a rate of $K/\Delta t$ instead of an ADC with rate $N/\Delta t$. For the physical implementation of the CS filters, we refer the reader to [28]-[30].

Figure 4 shows the channel occupancy evolution of Figure 3 recovered using the Gaussian measurement matrix, whereas Figure 5 shows the results obtained using the Spiky measurement matrix. In both cases K=N/2 and SNR=20dB.

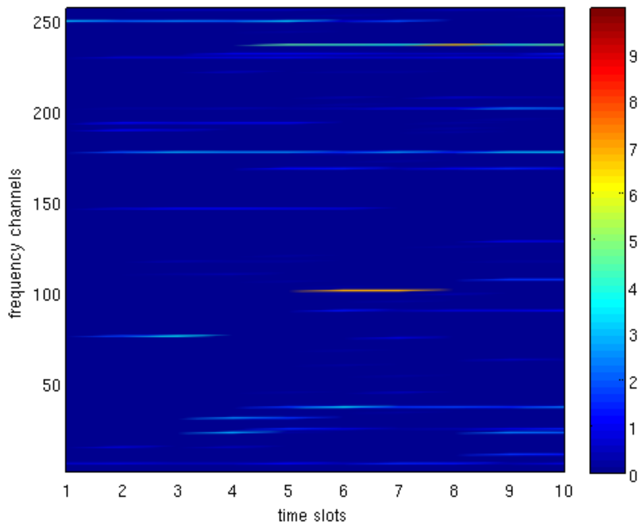

Figure 4 - Channel occupancy evolution recovered using the Gaussian measurement matrix, K=N/2.

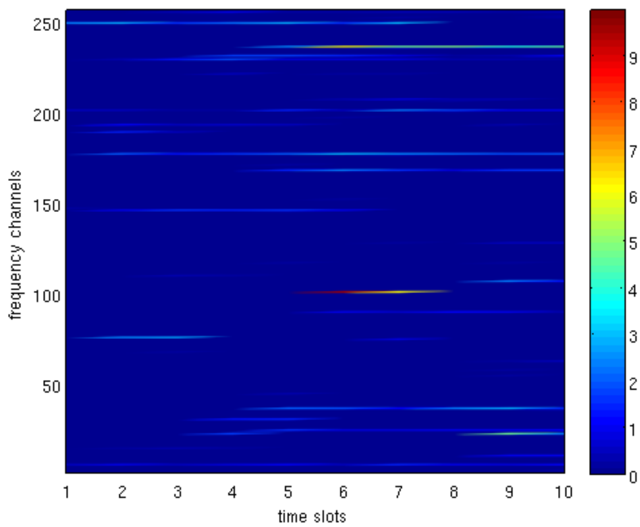

Figure 5 - Channel occupancy evolution recovered using the Spiky measurement matrix, K=N/2.

Figure 6 shows the Root Mean Square Error (RMSE) after the reconstruction of the channel occupancy signal. The RMSE measures the error in reconstructing $\mathbf{x}$ using CSS w.r.t. the reference signal estimated with all the N samples, that is

$$\mathrm{RMSE} = \sqrt{\frac{1}{MH}\sum_{h=1}^{H}\sum_{m=1}^{M}\left|\hat{\mathbf{x}}_m^{(h)} - \mathbf{x}_m^{(h)}\right|^2}\,, \tag{16}$$

where m and h are the time slot and the Monte Carlo run indexes, respectively.

The results are shown as a function of K (percentage of N) for both the measurements matrices and for different values of the Signal-to-Noise power ratio (SNR). The performance results obtained using the two matrices are about the same. It is also apparent that, in the absence of noise, it is possible to reconstruct the signal of interest using a very low number of samples (30% of N). However, as the noise power increases we need more samples to minimize the influence of the noise on the signal reconstruction. Anyway, when the SNR tends to be high, the signal can be almost perfectly reconstructed using fewer samples (40% of N). From our analysis (see Figures 5-6), the RMSE in reconstructing the signal is strictly related to the fact that, when the channel is busy, we need a high number of samples to reconstruct the whole spectrum with high precision. However, in this case, even if we use a low number of samples, a busy channel is always recognized to be busy. As a matter of fact, when performing the cognitive spectrum sensing function, we are not interested on reconstructing the whole spectrum with high accuracy, but rather on deciding which channels are busy. With regard to this latter operation, we apply the classical energy detector technique [31], which compares the squared value of each element of the spectrum occupancy vector $r_k = x_k^2$ with a threshold ζ to evaluate if the channel is busy/free. We evaluated the percentage of error in the decision on the channel occupancy applying the same threshold to the reconstructed signal as a function of K.

According to the signal model described in Section 2.2, in the two hypotheses the elements of the vector **x** are given by

$$\begin{cases} x_k \sim N(0, \sigma_{\mathbf{w}}^2), & H_0 \\ x_k \sim N(0, \sigma_{\mathbf{f}}^2 + \sigma_{\mathbf{w}}^2), & H_1 \end{cases} \tag{17}$$

where $\sigma_{\mathbf{f}}^2$ is the variance of the primary user's signal and $\sigma_{\mathbf{w}}^2$ is the variance of the noise. Being the squared value of a Gaussian r.v. a χ^2 r.v. with one degree of freedom, the binary hypothesis test is given by

$$\begin{cases} r_k \sim \sigma_{\mathbf{w}}^2 \chi_1^2 & H_0 \\ r_k \sim (\sigma_{\mathbf{f}}^2 + \sigma_{\mathbf{w}}^2)\chi_1^2 & H_1 \end{cases} \tag{18}$$

Indicating with P the upper incomplete gamma function, the probability of detection P_D and the probability of false alarm P_{FA} are given by

$$P_D = \Pr\{r_k \geq \zeta \mid H_1\} = \Pr\left\{\chi_1^2 \geq \frac{\zeta}{\sigma_{\mathbf{f}}^2 + \sigma_{\mathbf{w}}^2}\right\} = P\left(\frac{\zeta}{2\left(\sigma_{\mathbf{f}}^2 + \sigma_{\mathbf{w}}^2\right)}, \frac{1}{2}\right) \tag{19}$$

$$P_{FA} = \Pr\{r_k \geq \zeta \mid H_0\} = \Pr\left\{\chi_1^2 \geq \frac{\zeta}{\sigma_{\mathbf{w}}^2}\right\} = P\left(\frac{\zeta}{2\sigma_{\mathbf{W}}^2}, \frac{1}{2}\right). \tag{20}$$

In our Monte Carlo simulations, we evaluated the percentage of error in the decision on the channel occupancy (i.e. if a free channel is declared as busy and vice versa), the results are shown in Figure 7 when ζ is fixed for a probability of detection of 0.8. Note that in a radar detector the probability of false alarm is fixed to a desired value and the probability of detection is maximized according to the Newman-Pearson criterion. It is convenient to keep constant the probability of false alarm to a low value because a false alarm is more problematic than a miss detection. As a matter of fact, for each detection a lot of radar procedures, such as target tracking and target identification, are activated, if there are a lot of false alarms a great portion of the system memory and computational capabilities are occupied for the tracking of inexistent targets. For the problem of Spectrum Sensing, being the radar the secondary user of the channel, the more problematic event is the miss detection, that is when the channel is declared as free and the primary user is transmitting. For this reason, it is convenient to fix the probability of detection to a desired value and minimize the probability of false alarm. Note also that in this case, being the threshold dependent on the SNR, the probability of false alarm depends on the SNR. In particular, in the simulation the probability of detection has been fixed to 0.8 for each value of SNR, while the corresponding probability of false alarm according to (20) is 0.01 for SNR=20dB and 0.15 for SNR=15dB.

The results in Figure 7 show that, when the SNR is sufficiently high, the error percentage is reasonably low, which means that the busy/free decision can still be carried out on the signal reconstructed with few samples (<30% of N), even if the signal is not accurately reconstructed.

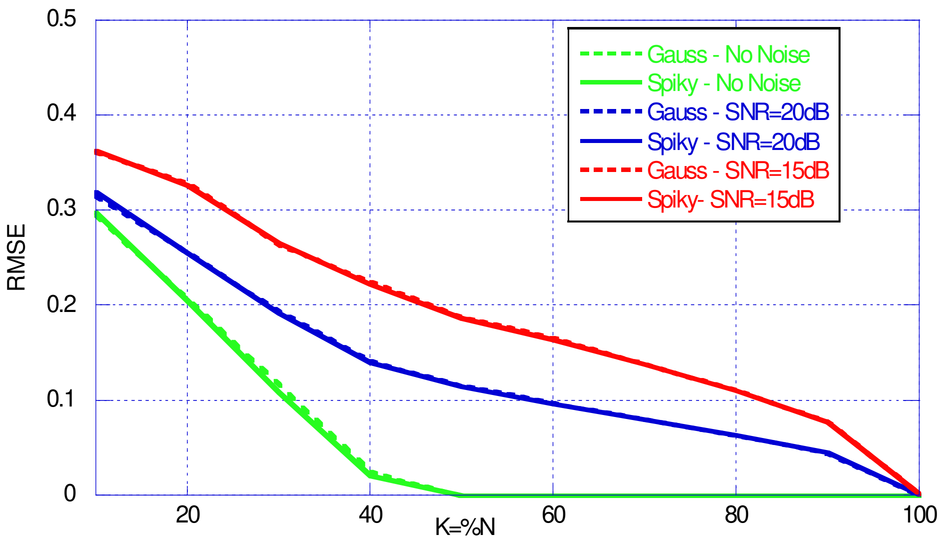

Figure 6 - RMSE for channel occupancy reconstruction as a function of K (percentage of N) for different SNR values.

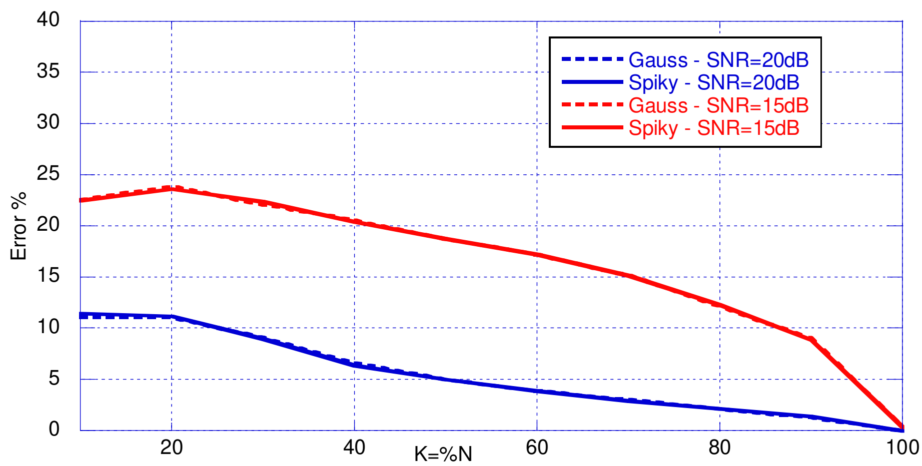

Figure 7 - Error percentage on the decision of channel occupancy as a function of K (percentage of N) for different SNR values.

4. Channel Monitoring for Spectrum Sharing

In the previous Section, we showed how the spectrum sensing detector exploits the received signal to obtain the observation symbols O_t used to evaluate if the channel is busy or free at time slot t. To detect the presence of the primary user, the spectrum sensing detector must process the time signal received in the whole time slot. Considering that the Pulse Repetition Interval (PRI) of the radar system and the time slot of the communication system are of the same time duration, in each channel at the time of transmitting (i.e. at the beginning of each PRI), the radar could not be able to measure if the frequency channel is effectively occupied by the communication system.

For minimizing interference to primary users while making the most out of the spectrum opportunities, the cognitive radar should keep track of variations in spectrum availability and, exploiting the history of the spectrum usage information, should make predictions of the future profile of the spectrum. Therefore, the cognitive radar system analyses the behaviour of the primary user in the frequency channel and, exploiting the time history of the channel occupancy (i.e. a sequence of observation symbols), it can evaluate the probability to have a spectrum opportunity at the beginning of each PRI, i.e. the probability that the monitored frequency channel is free at the time of transmitting.

In this Section, we describe how to estimate the channel parameters that model the behaviour of the primary user in a frequency channel and how to exploit this estimate to evaluate the probability to have a spectrum opportunity.

4.1 *Channel parameters estimation*

As discussed in Section 2.2, the statistical parameters that describe each frequency channel are the state transition probability matrix **A**, the emission probability matrix **B**, and the initial state distribution $\boldsymbol{\pi}=\{\pi_i\}$, defined as

$$\pi_i = \Pr\left[s_1 = S_i\right], \quad i=0,1. \tag{21}$$

Matrix **B** is related to the ROC of the spectrum sensing detector and, as discussed in Section 2.2, is assumed to be a-priori known. Hence, the problem of channel parameter estimation is to determine a method to estimate the model parameters **A** and $\boldsymbol{\pi}$ using a finite observation sequence $\boldsymbol{O}=[O_1...O_T]$ of T elements. The observation sequence used to adjust the model parameters is called training sequence since it is used to "train" the HMM. There is no way to solve analytically this problem [32]. In fact, given any finite observation sequence as training data, there is no optimal way of estimating the model parameters. However, the most widely adopted iterative procedure is the Baum-Welch method, which is closely related to the Expectation-Maximization (EM) method [23], [24], [32], [33]. The Baum-Welch method selects the parameters $\mathbf{A}$ and $\boldsymbol{\pi}$ such that $\Pr[\boldsymbol{O}|\mathbf{A},\boldsymbol{\pi}]$ is locally maximized.

In order to describe the iterative procedure for estimation of the HMM parameters, first we must define some useful variables. First consider the forward variable $\alpha_t(i)$ defined as

$$\alpha_t(i) = \Pr\left[O_1O_2...O_t, s_t = S_i \mid \mathbf{A}, \boldsymbol{\pi}\right] \tag{22}$$

That is the probability of the partial observation sequence $O_1...O_t$ and state S_i at time t, given the channel parameters $\mathbf{A}$ and $\boldsymbol{\pi}$. The forward variable can be inductively calculated initializing

$$\alpha_1(i) = \pi_i b_i(O_1), \quad i=0,1, \tag{23}$$

and iterating

$$\alpha_{t+1}(j) = \left[\sum_{i=0}^{1}\alpha_t(i)a_{ij}\right]b_j(O_{t+1}), \quad 1\le t\le T\text{-}1, j=0,1. \tag{24}$$

In a similar manner, the backward variable $\beta_t(i)$ is defined as

$$\beta_t(i) = \Pr\left[O_{t+1}O_{t+2}...O_T \mid s_t = S_i, \mathbf{A}, \boldsymbol{\pi}\right], \tag{25}$$

that is the probability of the partial observation sequence from t+1 to T, given state S_i at time t and the channel parameters $\mathbf{A}$ and $\boldsymbol{\pi}$.

Similarly, $\beta_t(i)$ can be solved inductively initializing

$$\beta_T(i) = 1, \quad i=0,1 \tag{26}$$

and iterating

$$\beta_t(i) = \sum_{j=0}^{1} a_{ij} b_j(O_{t+1}) \beta_{t+1}(j), \quad t=T\text{-}1,\dots,1;\ i=0,1. \tag{27}$$

Another important variable is the probability

$$\gamma_t(i) = \Pr\left[s_t = S_i \,|\, \boldsymbol{O}, \mathbf{A}, \boldsymbol{\pi}\right], \tag{28}$$

that is the probability of being in state S_i at time t, given the observation sequence $\boldsymbol{O}$ and the channel parameters $\mathbf{A}$ and $\boldsymbol{\pi}$. This probability can be expressed simply in terms of the forward-backward variables:

$$\gamma_t(i) = \frac{\alpha_t(i)\beta_t(i)}{\sum_{j=0}^{1} \alpha_t(j)\beta_t(j)}, \quad i=0,1. \tag{29}$$

Concluding, for the iterative estimation of the HMM parameter we must define the probability of being in state S_i at time t and state S_j at time t+1, given the observation sequence $\boldsymbol{O}$ and the channel parameters $\mathbf{A}$ and $\boldsymbol{\pi}$

$$\xi_t(i,j) = \Pr\left[s_t = S_i, s_{t+1} = S_j \,|\, \boldsymbol{O}, \mathbf{A}, \boldsymbol{\pi}\right], \quad i,j=0,1. \tag{30}$$

From the definitions of the forward and backward variables, we can write (30) in the form [32]:

$$\xi_t(i,j) = \frac{\alpha_t(i) a_{ij} b_j(O_{t+1}) \beta_{t+1}(j)}{\sum_{i=0}^{1}\sum_{j=0}^{1} \alpha_t(i) a_{ij} b_j(O_{t+1}) \beta_{t+1}(j)}, \quad i,j=0,1. \tag{31}$$

It is easy to verify by using (30) that the probability in (28) is given by

$$\gamma_t(i) = \sum_{j=0}^{1} \xi_t(i,j), \quad i=0,1. \tag{32}$$

If we sum $\gamma_t(i)$ over the time index t, we get a quantity which can be interpreted as the expected (over time) number of times that state S_i is visited, or equivalently, the expected number of transitions made from state S_i. Similarly, summation of $\xi_t(i,j)$ over t (from t=1 to t=T-1) can be interpreted as the expected number of transitions from state S_i to state S_j. Using (29) and (31) with the concept of counting event occurrences, it is possible to define a method to iteratively estimate the parameters of an HMM.

Considering that the ij–th element of the state transition probability matrix $\mathbf{A}$ can be considered as the ratio of the expected number of transitions from state S_i to state S_j and the expected number of transitions made from state S_i, it is possible to estimate the elements of $\mathbf{A}$ by using the following equation

$$\hat{a}_{ij} = \frac{\sum_{t=1}^{T-1} \xi_t(i,j)}{\sum_{t=1}^{T-1} \gamma_t(i)}, \quad i,j=0,1. \tag{33}$$

Similarly, the initial state distribution π_i can be considered as the expected number of times in state S_i at time t=1, therefore we can estimate $\boldsymbol{\pi}$ using

$$\hat{\pi}_i = \gamma_1(i), \quad i=0,1. \tag{34}$$

If we define the current channel parameters $\mathbf{A}$ and $\boldsymbol{\pi}$ and we use them to compute (29) and (31), and we define the re-estimated channel parameters as $\hat{\mathbf{A}}$ and $\hat{\boldsymbol{\pi}}$, determined from (33) and (34), then it has been proven in [34] and [35] that the model described by $\hat{\mathbf{A}}$ and $\hat{\boldsymbol{\pi}}$ is more likely than the model described by **A** and **π**, in the sense that $\Pr[\boldsymbol{O}|\hat{\mathbf{A}},\hat{\boldsymbol{\pi}}]>\Pr[\boldsymbol{O}|\mathbf{A},\boldsymbol{\pi}]$, i.e. we have found a new set of channel parameters from which the observation sequence is more likely to have been produced.

Based on the above procedure, if we iteratively use $\hat{\mathbf{A}}$ and $\hat{\boldsymbol{\pi}}$ in place of **A** and **π** and repeat the re-estimation, we can improve the probability of ***O*** being observed from the model until some limiting point is reached. The final result of this procedure is a maximum likelihood (ML) estimate of the HMM [32]. This procedure is called Baum-Welch method and it is summarized in Table 1.

Input: observation sequence $\boldsymbol{O}=O_1 \dots O_N$
initialize **A** and **π**
for k=1:MaxIter
calculate $\gamma_n(i)$ and $\xi_n(i,j)$ from **A** and **π**
estimate $\hat{\mathbf{A}}$ and $\hat{\boldsymbol{\pi}}$ from $\gamma_n(i)$ and $\xi_n(i,j)$
substitute **A** and **π** with $\hat{\mathbf{A}}$ and $\hat{\boldsymbol{\pi}}$.
end
Output: estimate of **A** and $\gamma_n(i)$, n=1,…N; i=0,1.

Table 1 - Baum-Welch procedure.

By Monte Carlo simulation, we evaluated that using 30 iterations the algorithm converges to a stable estimate of **A** and **π.** Figure 8 shows the Root Mean Square Error (RMSE) of the estimation of the elements of **A** as a function of the number of elements of the observation sequence T. These results have been obtained through 10^3 Monte Carlo runs by random generating a_{00} and a_{11} as independent and identically distributed (IID) random variables, uniformly distributed in [0,1]. Considering that (29) and (31) measure the expected number of transitions from one state to the other, it is clear that in order to have a good estimate of **A**, we need an high value of T, when the number of elements of the observation sequence is too low the estimate of **A** is biased.

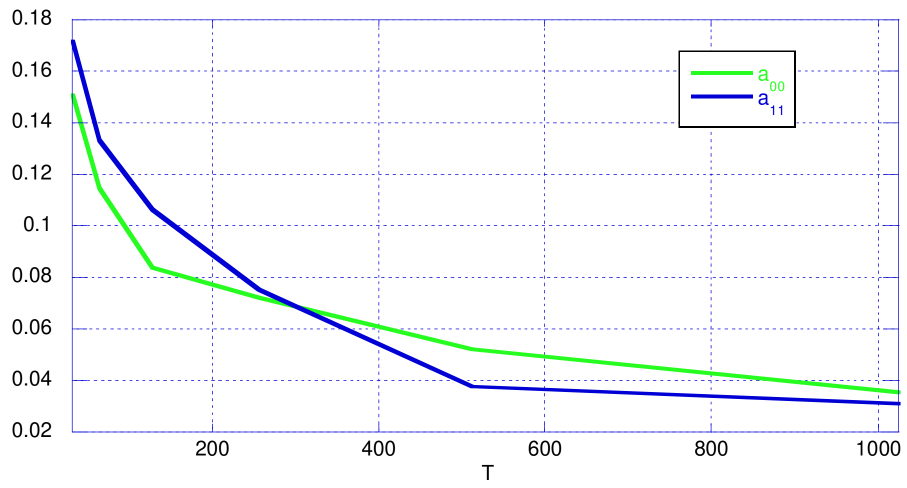

Figure 8 - RMSE in the estimation of **A** as a function of the number of elements of the observation sequence.

4.2 *Probability of Spectrum Opportunity*

In the previous Section, we showed how to estimate the channel parameters using a finite observation sequence. In this section, we show how the cognitive radar exploits these estimates to avoid interference with the primary user. We also show some simulation results that highlight how the proposed methodology can provide good radar performance in the presence of the user and low impact on the performance of the primary user by the presence of the radar.

As discussed, in the analysed scenario, at the time of transmitting the cognitive radar is not able to evaluate instantaneously if the operating channel is free or busy. However, using the channel parameter estimates obtained from the last T channel observations, the cognitive radar can calculate the probability that at the time of transmitting the channel is free, i.e. the probability to have a spectrum opportunity. If this probability is sufficiently high, the cognitive radar transmits, otherwise it does not transmit.

Figure 9 shows how the radar processes the continuous sequence of observations at the output of the spectrum-sensing detector. Since the estimation of A and $\gamma_t(i)$ is time consuming, the radar receiver performs these estimates using non-overlapping blocks of T elements, in each block the initialization is performed using the channel parameter estimates of the previous block. As showed in Figure 9, the channel parameter estimates performed in each block are used to evaluate the probability to have a spectrum opportunity using a sliding window that collects the last T observations received in the previous time slots.

There are T sliding windows for each block, in particular in the k-th sliding window, using the estimate of **A** and fixing $\pi_i=\gamma_k(i)$, the signal processor of the radar evaluates the forward and the backwards variables using (23)-(27). Therefore, similarly to (29), evaluates the probability that the last observation in the sliding window corresponds to the channel state S_i, that is

$$\gamma(i) = \frac{\alpha_T(i)\beta_T(i)}{\sum_{j=0}^{1}\alpha_T(j)\beta_T(j)}, \quad i=0,1. \tag{35}$$

This probability is used to evaluate the probability to have a spectrum opportunity:

$$p_{SO} = \gamma(0)a_{00} + \gamma(1)a_{01}, \tag{36}$$

i.e. the probability that in the previous time slot the channel was free and in the current time slot it remains free plus the probability that in the previous time slot the channel was busy and in the current time slot it becomes free. The signal processor compares the probability to have a spectrum opportunity with a threshold λ, and transmits only if the probability is greater than λ.

There are two kinds of errors. The first one, e_0, is the event in which the cognitive radar does not transmit and the channel is free, i.e. the probability to lose a spectrum opportunity. The other kind of error, e_1, is the case in which the radar transmits and the channel is occupied by the primary user, i.e. the probability to have a collision.

Figure 10 shows the probability of these two errors as a function of the threshold λ, this graph can be used to tune the cognitive radar to the desired performance. These results have been obtained through 10^3 Monte Carlo runs by random generating a_{00} and a_{11} as independent random variables uniformly distributed in the range [0,1].

It is clear that when threshold λ is zero, the radar is always transmitting, therefore the probability of e_1 coincides with the probability that the channel is busy, that for the matrix **A** that we used in our simulation, is 0.5. Similarly, when the threshold λ is one, the radar never transmits and the probability of e_0 coincides with the probability that the channel is free, that in our particular case, is 0.5.

Figure 11 shows the probability to lose a spectrum opportunity and the probability to have a collision as a function of time, observing the performance of the system for 9246 time slots (i.e. 9 blocks of 1024 elements). These results have been obtained through 10^3 Monte Carlo runs, generating a_{00} and a_{11} as IID random variables uniformly distributed in [0,1] and fixing the threshold λ to 0.65.

The simulation results show how the performance of a cognitive radar that adopts the proposed methodology are constant during the time and much better than the performance of the non cognitive radar that always transmits ignoring the presence of the primary user and than the radar that never transmits to avoid interference with the primary user of the channel.

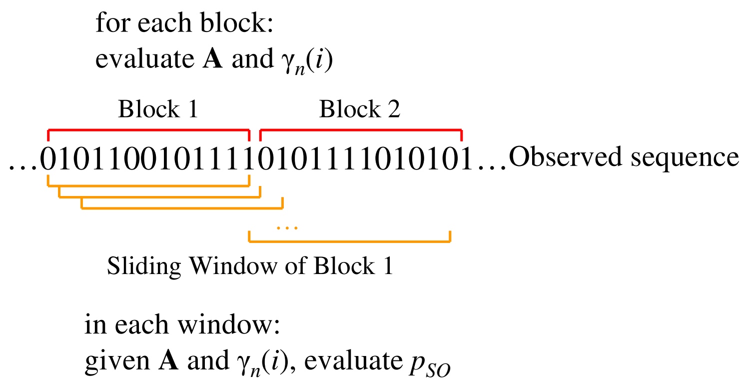

Figure 9 - How to process the observed sequence.

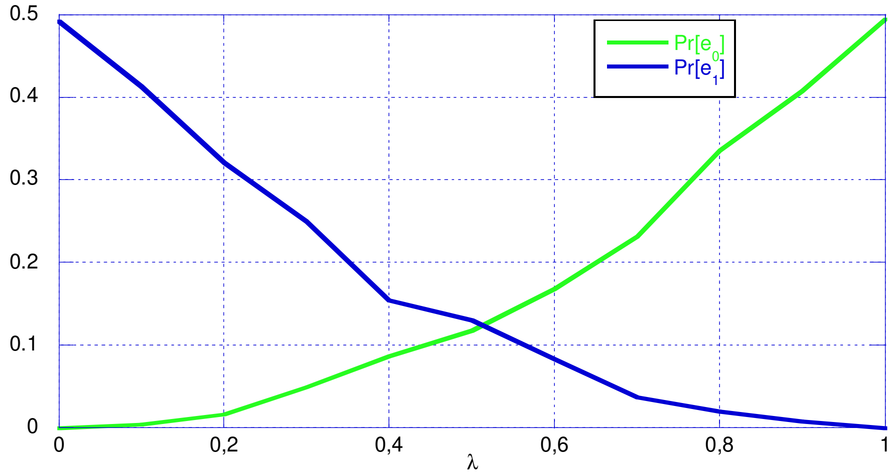

Figure 10 - Probabilities of e_0 and e_1 as a function of λ.

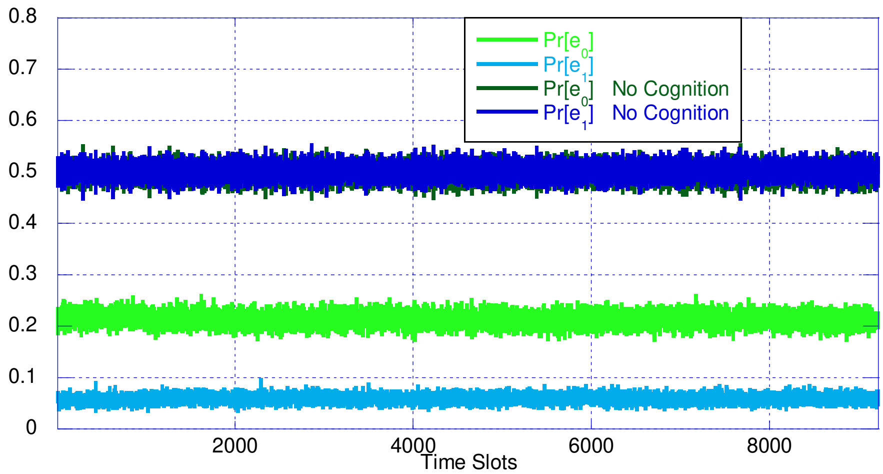

Figure 11 - Probabilities of e_0 and e_1 as a function of time.

5. Conclusions

Since the availability of frequency spectrum for radar sensors continuously diminished and fragmented, next generation radar systems should be able to operate in spectrally dense environments, coexisting with other systems operating in the same frequency channel. For this reason, an important system requirement is the ability to recognize and react to the behaviour of other users radiating in the same operational environment that, in turn, leads to the need of new methodologies and techniques, based upon cognition as enabling technology. The cognitive methodology to reduce mutual interference between the radar and the other radiating elements is based on two main concepts: Spectrum Sensing, that has the goal to recognize the frequencies used by other systems using the same spectrum in real time, and Spectrum Sharing, that has the goal to limit interference from the radar to other services and vice versa.

This chapter focuses on two main topics, the role that Compressed Sensing in Spectrum Sensing and the problem of channel parameter estimation for Spectrum Sharing. In particular, we demonstrate that CS techniques can provide a significant reduction in acquisition time, reducing the cost for high resolution Analog-to-Digital converters with large dynamic range and high speed signal processors. In the specific application, where the goal is not reconstructing the whole spectrum with high accuracy, but rather to decide which are the busy channels in the considered band, the results show that, when the SNR is sufficiently high, the error percentage on the busy/free decision can be low already using less than 30% of the total samples of the original signal. This mitigates the hardware constraints of conventional spectrum sensing techniques and allows to reduce the sampling rate. Moreover, this paper describes a technique to estimate the channel parameters that model the behaviour of the primary user of the channel, and propose a cognitive method that, exploiting these estimates, enables a radar to operate in a spectrally dense environment. The performance of the cognitive radar is evaluated in terms of probability to lose a spectrum opportunity and probability to have a collision with the primary user of the channel. The numerical results suggest that the proposed cognitive algorithm lowers the mutual interference between the radar and the primary users.

REFERENCES

[1] M. Wicks, “Spectrum crowding and Cognitive Radar,” *2nd International Workshop on Cognitive Information Processing* (CIP2010), Elba Island, Italy, June 2010.

[2] M. Wicks, “Cognitive radar: A way forward,” *IEEE International Radar Conference* (RADAR 2011), May 2011.

[3] ITU-R Resolution 229, “Use of the bands 5150-5250 MHz, 5250-5350 MHz and 5470-5725 MHz by the mobile service for the implementation of wireless access systems including radio local area networks”, 2012.

[4] ITU-R RECOMMENDATION M.1652, “Dynamic frequency selection (DFS) in wireless access systems including radio local area networks for the purpose of protecting the radio determination service in the 5 GHz band”, 2003.

[5] U.S. Department of Commerce, “An Assessment of the Near-Term Viability of Accommodating Wireless Broadband Systems in the 1675-1710 MHz, 1755-1780 MHz, 3500-3650 MHz, and 4200-4220 MHz, 4380-4400 MHz Bands”, 2010.

[6] E. Obregon, K.W. Sung, J. Zander, “Secondary Access to the Radar Spectrum Bands: Regulatory and Business Implications”, *24th European Regional Conference of the International Telecommunications Society*, Florence, Italy, 2013.

[7] S. Haykin, “Cognitive radar: A way of the future,” *IEEE Signal Process. Mag.*, Vol. 23, No. 1, pp. 30-40, Jan. 2006.

[8] S. Haykin, X. Yanbo, P. Setoodeh, “Cognitive Radar: Step toward Bridging the Gap between Neuroscience and Engineering,” *Proceedings of the IEEE*, vol.100, no.11, pp.3102-3130, Nov. 2012

[9] S. Haykin, *Cognitive Dynamic Systems: Perception-action Cycle, Radar and Radio*, Cambridge University Press, 2012.

[10] G.T. Capraro, A. Farina, H. Griffiths, M.C. Wicks, “Knowledge-based radar signal and data processing: a tutorial review,” *IEEE Signal Process. Mag.*, Vol. 23, No. 1, pp. 18-29, Jan. 2006.

[11] P. Stinco; M. Greco; F. Gini; M. Rangaswamy; “Ambiguity function and Cramer-Rao bounds for universal mobile telecommunications system-based passive coherent location systems,” *Radar, Sonar & Navigation, IET*, vol.6, no.7, pp.668-678, August 2012

[12] P. Stinco; M. Greco; F. Gini; A. Farina; "Posterior Cramér-Rao Lower Bounds for Passive Bistatic Radar Tracking with Uncertain Target Measurements" *Special Issue on Sensor Array Processing, Signal Processing, Signal Processing*, Vol. 93, No. 12, pp. 3528-3540, December 2013.

[13] Y. Hur, J. Park, W. Woo, K. Lim, C. Lee, H. Kim, J. Laskar, "A wideband analog multi-resolution spectrum sensing (MRSS) technique for cognitive radio (CR) systems," *in Proc. IEEE Int. Symp. Circuits and Systems*, Island of Kos, Greece, May 2006, pp. 4090–4093.

[14] Y. Yuan, P. Bahl, R. Chandra, P. A. Chou, J. I. Ferrell, T. Moscibroda, S. Narlanka, Y. Wu, "KNOWS: Cognitive radio networks over white spaces," *in Proc. IEEE Int. Symposium on New Frontiers in Dynamic Spectrum Access Networks*, Dublin, Ireland, Apr. 2007, pp. 416–427.

[15] E.J. Candes, M.B. Wakin; "An Introduction To Compressive Sampling," *Signal Processing Magazine, IEEE*, Vol. 25, No. 2, pp. 21-30, March 2008.

[16] D.L. Donoho; "Compressed sensing," *Information Theory, IEEE Transactions on*, Vol. 52, No. 4, pp. 1289-1306, April 2006.

[17] D.L. Donoho, X. Huo; "Uncertainty principles and ideal atomic decomposition," *Information Theory, IEEE Transactions on*, Vol. 47, No. 7, pp. 2845-2862, Nov 2001.

[18] Federal Communications Commission, Notice of Inquiry and Notice of Proposed Rulemaking: In the matter of Establishment of an Interference Temperature Metric to Quantify and Manage Interference and to Expand Available Unlicensed Operation in Certain Fixed, Mobile and Satellite Frequency Bands, ET Docket No. 03-237; November 28, 2003.

[19] D. Cabric, S. Mishra, R. Brodersen, "Implementation issues in spectrum sensing for cognitive radios," *in Proc. Asilomar Conf. on Signals, Systems and Computers*, Vol. 1, Pacific Grove, California, USA, Nov. 2004, pp. 772–776.

[20] P. Kolodzy "Dynamic Spectrum Policies: Promises and Challenges", *CommLaw Conspectus*, 2004.

[21] T. Clancy, "Formalizing the interference temperature model", *Wiley Journal on Wireless Communications and Mobile Computing*, 7 (9): 1077-1086, 2007.

[22] J. Bater; H. Tan; K.N. Brown; L. Doyle, "Modelling Interference Temperature Constraints for Spectrum Access in Cognitive Radio Networks," *IEEE International Conference on Communications* (ICC 2007), pp. 6493-6498, 24-28 June 2007.

[23] M. Sharma; A. Sahoo; K.D. Nayak, “Channel modeling based on interference temperature in underlay cognitive wireless networks,” *IEEE International Symposium on Wireless Communication Systems* (ISWCS 2008), pp.224-228, 21-24 Oct. 2008.

[24] S.D. Barnes; B.T. Maharaj, “Performance of a Hidden Markov channel occupancy model for cognitive radio,” *AFRICON*, 2011, pp.1-6, 13-15 Sept. 2011.

[25] T. Yucek, H. Arslan, “A survey of spectrum sensing algorithms for cognitive radio applications”, *IEEE Communication Surveys & Tutorials*, 11 (1): 116-130, 2009.

[26] R.G. Baraniuk, “Compressive Sensing [Lecture Notes],” *Signal Processing Magazine, IEEE* , Vol. 24, No. 4, pp.118-121, July 2007.

[27] S.S. Chen, D.L. Donoho, M.A. Saunders; “Atomic decomposition by basis pursuit”, *SIAM Journal on Scientific Computing*, 20 (1998), pp. 33-61.

[28] M.A. Davenport, P.T. Boufounos, M.B. Wakin, R.G. Baraniuk, “Signal Processing With Compressive Measurements,” *IEEE Journal of Selected Topics in Signal Processing,* Vol. 4, No. 2, pp. 445-460, April 2010.

[29] J.A. Tropp, J.N. Laska, M.F. Duarte, J.K. Romberg, R.G. Baraniuk, “Beyond Nyquist: Efficient Sampling of Sparse Bandlimited Signals,” *IEEE Transactions on Information Theory*, Vol. 56, No. 1, pp. 520-544, Jan. 2010.

[30] Y.C. Eldar, G. Kutyniok, *Compressed Sensing*, Cambridge University Press, June 2012.

[31] Q. Zhao, B.M. Sadler, “A survey of dynamic spectrum access: signal processing, networking, and regulatory policy”, *IEEE Signal Processing Mag*., Vol. 4, No. 3, pp. 79-89, May 2007.

[32] L. Rabiner, “A tutorial on hidden Markov models and selected applications in speech recognition,” *Proceedings of the IEEE*, Vol. 77, No. 2, pp.257-286, Feb 1989.

[33] A.P. Dempster, N.M. Laird, D.B. Rubin, “Maximum likelihood from incomplete data via the EM algorithm”, *J. Roy. Stat. Soc.*, Vol. 39, No. 1, pp. 1-38, 1977.

[34] L.E. Baum, G.R. Sell, “Growth functions for transformations on manifolds”, *Pac. J. Math*., Vol. 27, No. 2, pp. 211-227, 1968.

[35] J.K. Baker, “The dragon system-An overview”, *IEEE Trans. Acoust. Speech Signal Processing*, Vol. ASP-23, No. 1, pp. 24-29, Feb. 1975.

CHAPTER 2

COGNITIVE PASSIVE TRACKING IN SYMBIOTIC IEEE 802.22 COMRADE SYSTEMS

ABSTRACT

This chapter deals with a Symbiotic Radar, defined as a Passive Radar that is an integral part of a communication network. The Symbiotic Radar is integrated with an IEEE 802.22 WRAN and linked with the Base Station. It can work as a purely passive radar or, and this is the novelty in the system, can use the Base Station to suggest the best Customer Premise Equipment that should be scheduled for transmission to improve tracking performance. This paper defines a cognitive passive tracking algorithm that exploits the feedback information contained in the target state prediction to improve the performance while preserving the communication capabilities of the complete network.

1. Introduction

Communication systems are proliferating at incredible rates, resulting in a spectrally dense environment and fierce competition for frequency bands that traditionally had been exclusively allocated to radar systems as primary legal users. To cope with the issue of spectrum crowding, future radar systems, as well as communication systems, should be based upon cognitive radio technology to coexist with other radiating systems anticipating their behavior and properly reacting to avoid interference 1-3.

Moreover, for both communication and radar systems, an increasing number of functions, traditionally realized by hardware components, are being replaced by digital signal processing and the resulting radio frequency (RF) front-end architectures of these systems have become more and more similar. This offers the possibilities to design symbiotic systems, where communication and radar applications could be realized exploiting the same transmitted waveform 4, 5.

This work deals with a Symbiotic Radar (SR) integrated with an IEEE 802.22 WRAN (Wireless Regional Area Network). The radar receiver is based on passive radar technology and exploits the IEEE 802.22 devices as transmitters of opportunity. Being integrated with the WRAN, the SR can select some of these transmitters to improve radar performance.

The IEEE 802.22 is a new standard 6 based on Cognitive Radio techniques for WRAN that exploits, in a non-interfering and opportunistic basis, the unused channels in the VHF and UHF bands allocated to television. In this manner, the occupied spectrum is used very efficiently for both radar and communication functionalities that can be operated simultaneously, which guarantees a permanent availability of both functions and helps to overcome the limited availability of spectral resources.

The architecture of the IEEE 802.22 network is composed of a Base Station (BS) that covers a cell with a radius up to 30 km, providing high-speed internet service for up to 512 fixed or portable Customer Premise Equipment (CPE) devices or groups of devices.

The definition of SR has been recently introduced in patent in 7 and in the related work 8, where a passive radar is an integrated commensal function of an IEEE 802.22 Base Station. The radar exploits the signal arising from several BS sharing the spectrum with the communication system in a collaborative way. In this work the definition of symbiotic radar is different and new. In particular, we assume that SR exploits the signals arising from a single BS and the CPEs of the WRAN. Moreover, the radar system is defined as symbiotic since it can control the Medium Access Control (MAC) layer of the WRAN selecting, in a collaborative way with the BS, some of the CPEs that must be scheduled to transmit in each frame to improve radar performance.

Some recent works 8-13 analyzed how the possibility to exploit IEEE 802.22 devices as transmitters of opportunity for Passive Radar (PR) systems. In particular, 8 and 11 study a PR, defined as commensal radar, which exploits the signals of opportunity arising from several IEEE 802.22 Base Station focusing also on the foliage penetration capabilities in UHF/VHF frequency bands. On the other hand, works 12 and 13 analyze a PR that combines the signals of opportunity of a single BS and the CPEs for target detection and target parameter estimation, respectively.

The SR described in this work exploits the signal emitted by the BS and the CPEs for surveillance purposes, but it is also linked to the BS to suggest the best CPEs that should be scheduled for transmission to improve target tracking performance. In particular, the IEEE 802.22 WRAN is composed of collaborative CPEs, including computers, portable devices, but also wireless or infrared cameras that can also be used for surveillance purposes. The SR can also be considered as a CPE that provides full surveillance coverage day and night, and in all weather conditions, using radar technology. The complete radar system, which is integrated in the communication network, can be defined as a ComRadE system, where Com stands for communication, Rad stands for radar, while the whole word ComRadE indicates that the communication and the radar systems are “friends” or “allies”. In such a system, the CPEs, belonging to a communication WRAN that has also radar surveillance capabilities, are assumed to be collaborative and, if scheduled to transmit by the SR and the BS, emit their data stream to improve radar performance. Note also that similarly to conventional passive radar, the SR does not process the information contained in the data emitted by the BS and the CPEs, but exploits only their emitted physical signals.

The main advantage of a symbiotic ComRadE system that exploits the IEEE 802.22 standard is that the complete system can be installed anywhere, without any license to transmit and without interfering with other radiating systems. Actually, the SR is passive and does not involve any radar transmitter hardware, and the IEEE 802.22 standard is based on cognitive radio techniques. Moreover, both the SR and the IEEE 802.22 devices are very low power consuming systems that can be powered with solar panel or small wind turbines 14. For this reason, the complete system can be installed in remote areas where the electricity grid is inexistent or dated and fragile.

As mentioned, the SR is linked to the BS and suggests the best CPEs that must be scheduled to transmit in order to improve target tracking performance. This concept is directly linked to the cognitive tracking algorithm introduced by Haykin in 15 and 16. Exploiting the perception-action cycle, the receiver feeds the transmitter with feedback information that is processed to select the best transmitted waveform. In the particular case of a passive radar that exploits signals of opportunity emitted by the BS and the CPEs, its performance is dependent on the position of the target with respect to the location of the transmitters and the receiver (bistatic geometry). Hence, the feedback information contained in the target state prediction stage can be exploited for the selection of the best transmitters of opportunity. Over the years, a multitude of filters have been proposed for target tracking 17. In this paper, we consider the Extended Kalman Filter (EKF), combined with a cognitive algorithm for the selection of the best set of CPEs.

In our previous works 18,19 we studied the selection of the best transmitter of opportunity in a multistatic radar system, that minimizes the range and target velocity measurement errors. In this paper, these results are used to initialize the search for the best set of illuminators of opportunity that must be exploited to minimize the mean square error of target state prediction along the target trajectory, in terms of target position and target velocity in the Cartesian plane. With respect to our previous works, where the PR was not linked with the transmitters of opportunity, in this paper we introduce a cognitive algorithm for the selection of the CPEs that exploits the perception-action cycle performed by the SR and the linked BS. The perception is made by the SR that, starting from the a-priori knowledge of the CPEs that guarantees the best measurement 18, 19, minimizes a predefined cost function on the target state estimation to select a subset of CPEs which are scheduled to transmit by the BS (action).

The proposed algorithm is designed such that the communication capabilities of the complete network are preserved. Numerical results show that the proposed cognitive tracking algorithm improves the performance of the symbiotic radar while preserving the communication capabilities of the ComRadE system.

2. IEEE 802.22 emitted signals and analyzed scenario

The IEEE 802.22 emitters operate in the white space bands of the TV signal in the frequency range of 54~862 MHz. The standard specifies three operating modes depending on the channel bandwidth: 6 MHz, 7 MHz, and 8 MHz. Without loss of generality, we consider here the 6 MHz based channel case.

The transmitted signal is based on an OFDMA scheme where information to or from multiple CPEs is modulated on orthogonal sub-carriers using the Inverse Fast Fourier Transform (IFFT) of size N=2048. In the 6 MHz based channel mode, the sampling frequency f_S is 6.856 MHz, the sub-carriers are divided in 60 sub-channels and the sub-carrier spacing Δf is $\Delta f = f_S/N$=3347.656 Hz.

In an IEEE 802.22 cell, a single BS controls the medium access and manages multiple CPEs. The timeline is divided into super-frames of time duration 160 msec. Each super-frame is composed of 16 frames of 10 msec, each of which is composed of two parts: a downstream (DS) sub-frame, where the BS transmits and the CPEs receive, and an upstream (US) sub-frame, where the M scheduled CPEs transmit to the BS. The time/frequency frame structure is depicted in Fig. 12, the DS and the US sub-frames are divided by the Transmit/Receive Transition Gap (TTG), a time gap to allow the CPE to switch between the receive mode and the transmit mode and to absorb the signal propagation time for a distance of up to 30 km. The vertical axis in Fig. 12 is the frequency domain composed of 60 sub-channels while the horizontal axis is the time domain, each horizontal time slot is an OFDM symbol. The first symbol in the DS sub-frame is composed of a frame preamble and the headers 6, the following symbols are for the downstream payload. Note that the BS transmits, exploiting all the 60 sub-channels and the data bursts are laid vertically.

In the US sub-frame, each burst is mapped horizontally, OFDM symbol by OFDM symbol, in the same logical sub-channel. In the upstream direction, each CPE can occupy one or more sub-channels transmitting at least 7 OFDM symbols. According to the standard 6, the signal emitted during the h^{th} OFDM symbol is given by the IFFT of size N=2048 of the sequence $c_h^{(m)}[f]$, that is

$$s_h^{(m)}[n] = \frac{1}{|\Omega_m|} \sum_{f \in \Omega_m} c_h^{(m)}[f] e^{j2\pi fn/N}, \tag{37}$$

where the index m is the m^{th} transmitter, i.e. m=0 is for the BS while m=1,2,..,M are for the M CPEs scheduled to transmit in the US sub-frame. According to the standard, the number M can change in each frame and up to M=16 can be scheduled to transmit in each US sub-frame. In this work and loss of generality, we assume that M is constant and has been fixed to M=8 (see Fig. 12).

In (1), Ω_m is the set of sub-carrier frequencies allocated to the m^{th} transmitter according to Fig. 12 and $|\Omega_m|$ is the size of Ω_m.

The complex number $c_h^{(m)}[f]$ specifies a point in a QAM constellation 6 and it is the data transmitted by the m^{th} emitter on the sub-carrier whose frequency offset index is f, during the h^{th} symbol. Clearly $c_h^{(m)}[k]$ is null in the sub-carriers that are not assigned to the transmitter.

Fig. 13 shows the IEEE 802.22 WRAN scenario analyzed in this work. The network is composed by a BS that provides internet access to 32 CPEs. The SR is not co-located with the BS and can control the BS to select the best cooperative CPEs that must be scheduled to improve target tracking performance. The figure also shows the target trajectory in the absence of process noise. Clearly, the position of the CPEs may be different in other configurations and in general is not symmetric with respect to the BS. Moreover, considering that the standard has also been designed for portable devices, the position of the CPEs can change in time. We consider fixed positions of the CPEs during the target tracking to highlight the dependence of the performance on the position of the target along the target trajectory with respect to the locations of the transmitters of opportunity. Moreover, in the simulation section we also consider the scenario consisting of 256 CPEs whose positions have been randomly chosen in the surveillance area.

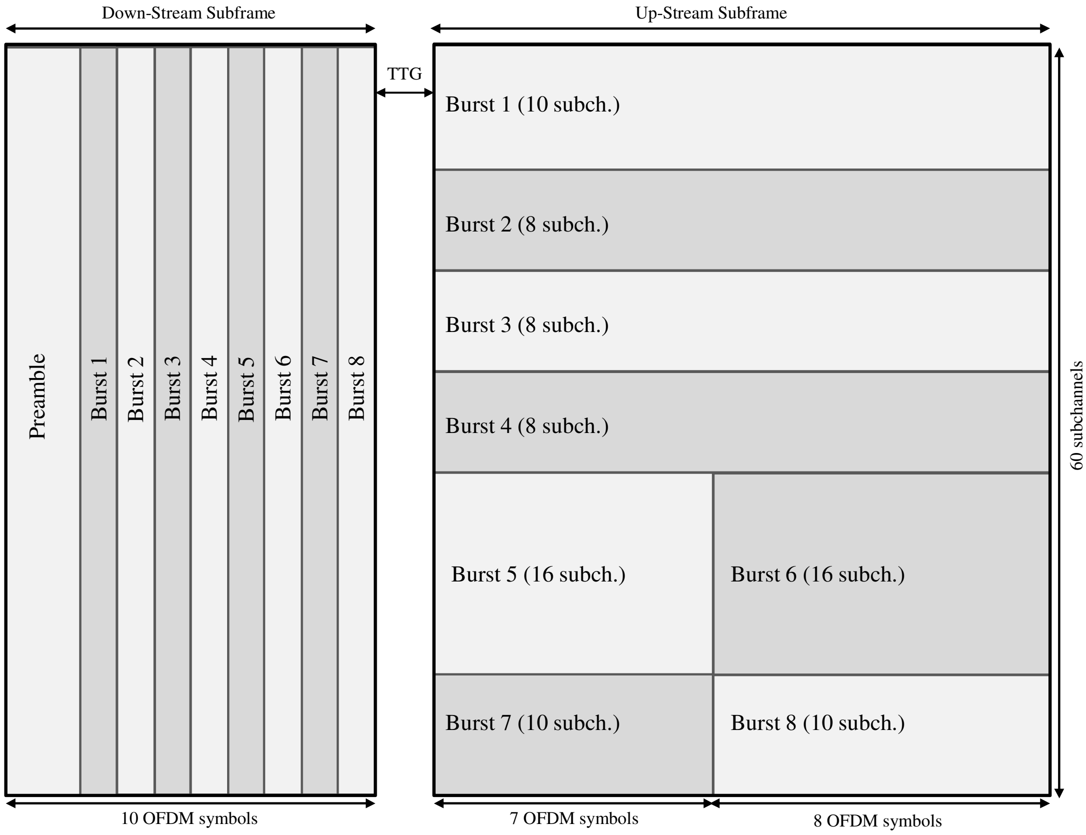

Fig. 12 – Time/frequency structure of a frame.

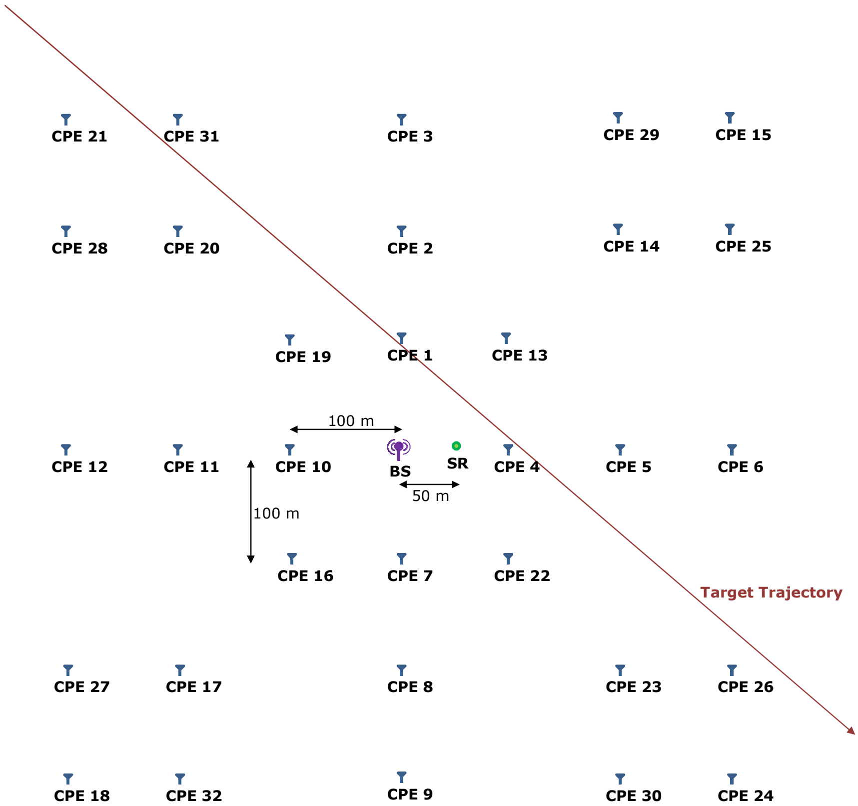

Fig. 13 – Analyzed Scenario.

3. Cognitive passive tracking

Let the state vector be defined as $\mathbf{x}_k=[x_k \ \dot{x}_k \ y_k \ \dot{y}_k]^T$, where (x_k, y_k) is the location of the target, assumed to be on the x-y plane, and $(\dot{x}_k, \dot{y}_k)$ is the target velocity vector. Assume now that the target motion equation is described by the following dynamic state 20

$$\mathbf{x}_k = \mathbf{F}\mathbf{x}_{k-1} + \mathbf{n}_{k-1}, \tag{38}$$

$$\mathbf{F} = \begin{bmatrix} 1 & T & 0 & 0 \\ 0 & 1 & 0 & 0 \\ 0 & 0 & 1 & T \\ 0 & 0 & 0 & 1 \end{bmatrix}, \tag{39}$$

where T is the super-frame duration and $\mathbf{n}_k$ models the process noise, which takes into account mis-modeling effects or unforeseen disturbance in the target motion. The process noise vector $\mathbf{n}_k$ is assumed to be a zero-mean Gaussian distributed, with covariance matrix 20:

$$\mathbf{Q} = q\begin{bmatrix} T^3/3 & T^2/2 & 0 & 0 \\ T^2/2 & T & 0 & 0 \\ 0 & 0 & T^3/3 & T^2/2 \\ 0 & 0 & T^2/2 & T \end{bmatrix}, \tag{40}$$

where q is a deterministic parameter which takes into account the process noise power.

Exploiting the target echoes arising from the target which is illuminated by the BS and the M scheduled CPEs in each frame, the SR is able to measure the ranges and the bistatic velocities for the M+1 transmitter-target-receiver paths, as described in 12,13.

The available measurements at time k are collected in the column vector $\mathbf{z}_k=[r_k^{(0)}\ \zeta_k^{(0)}\ \ldots\ r_k^{(M)}\ \zeta_k^{(M)}\ \theta_k]^T$, whose components are the range from receiver to target $r_k^{(0)}$ and the bistatic velocity $\zeta_k^{(0)}$, obtained by exploiting the signal emitted by the BS in the DS, the set of ranges $\{r_k^{(1)},\ldots, r_k^{(M)}\}$, and bistatic velocities $\{\zeta_k^{(1)},\ldots, \zeta_k^{(M)}\}$ obtained by exploiting the M CPEs in the US and the Direction of Arrival (DOA) of the target echo θ_k.

The relationship between the measurement vector and the target state is given by

$$\mathbf{z}_k = \mathbf{h}_k\left(\mathbf{x}_k\right) + \mathbf{w}_k . \tag{41}$$

The explicit expression of $\mathbf{h}_k(\mathbf{x}_k)$ is reported in Appendix A; $\mathbf{w}_k$ is the measurement noise, which is independent of the process noise $\mathbf{n}_k$. The measurement noise vector is assumed to be Gaussian distributed with zero mean and covariance matrix $\mathbf{R}_k$.

In bistatic radar systems, it is well known that the accuracy of the estimates of range and bistatic velocity heavily depend on the geometry of the scenario, i.e. the position of the target with respect to the radar receiver and the transmitter of opportunity that is exploited, as well as on the signal to noise ratio (SNR), which is itself dependent on the geometry 18,19. The expression of $\mathbf{R}_k$ is reported in Appendix B. Note that this covariance matrix is a function of time since the bistatic geometry changes along the target trajectory. As discussed, to estimate the state vector $\mathbf{x}_k$ from the measurements $\mathbf{z}_k$, we use the EKF, where the target state estimates are computed recursively as follow 17:

$$\hat{\mathbf{x}}_{k|k} = \hat{\mathbf{x}}_{k|k-1} + \mathbf{G}_k \left(\mathbf{z}_k - \mathbf{h}_k \left(\hat{\mathbf{x}}_{k|k-1} \right) \right), \tag{42}$$

$$\hat{\mathbf{x}}_{k|k-1} = \mathbf{F} \hat{\mathbf{x}}_{k-1|k-1}, \tag{43}$$

$$\mathbf{P}_{k|k} = \mathbf{P}_{k|k-1} + \mathbf{G}_k \mathbf{S}_k \mathbf{G}_k^T, \tag{44}$$

$$\mathbf{P}_{k|k-1} = \mathbf{Q} + \mathbf{F} \mathbf{P}_{k-1|k-1} \mathbf{F}^T, \tag{45}$$

$$\mathbf{S}_k = \hat{\mathbf{H}}_k \mathbf{P}_{k|k-1} \hat{\mathbf{H}}_k^T + \mathbf{R}_k, \tag{46}$$

$$\mathbf{G}_k = \mathbf{P}_{k|k-1} \hat{\mathbf{H}}_k^T \mathbf{S}_k^{-1}, \tag{47}$$

where $\hat{\mathbf{H}}_k$ is the matrix obtained by the linearization of the non-linear function $\mathbf{h}_k(\mathbf{x}_k)$ and is defined as the Jacobian evaluated at $\hat{\mathbf{x}}_{k|k-1}$:

$$\hat{\mathbf{H}}_k = \left[\nabla_{\mathbf{x}_k} \mathbf{h}_k^T \left(\mathbf{x}_k \right) \right]^T \Big|_{\mathbf{x}_k = \hat{\mathbf{x}}_{k|k-1}}. \tag{48}$$

The explicit expression of $\hat{\mathbf{H}}_k$ is given in Appendix A.

Now let us consider how the perception-action cycle concept defined by Haykin in 15 can be applied for cognitive passive tracking. The perception-action cycle is the fundamental function of a cognitive tracker. For active radar systems, at each step k, the transmitter modifies the transmitted signal (action) minimizing a specific cost function that depends on the feedback information. This information is evaluated by the receiver and provides a compressed measure of information contained in the radar returns (perception).

Clearly, a passive radar does not have any radar transmitter on its own and hence it is not able to modify the transmitted signal. However, the Symbiotic Radar is integrated with the communication network and hence it can control the BS to select the CPEs that guarantee the best performance for target state estimation. In other words, similarly to cognitive active radars that select the best transmitted waveform, the SR exploits the feedback information to select the best transmitters of opportunity that minimize a pre-defined cost function. This concept was originally introduced in 18 and 19. In particular, in these papers we describe how to exploit the Cramér-Rao Bounds (CRB) of range and bistatic velocity, which depend on the geometry and are strictly related to the measurement covariance matrix $\mathbf{R}_k$, to select the best transmitters of opportunity. The CRB can be evaluated off-line and, exploiting this information, for each point of the surveillance area, the SR knows which of the CPE provides the minimum measurement errors.

Fig. 14 shows the best CPE for each point of the surveillance area depicted in Fig. 13. The color scale in quantized into 32 levels, each of which is associated with one of the 32 CPEs of the analyzed scenario. The index associated with each CPE are those depicted also in Fig. 13. Note that for each point, the best transmitter is the closest to the target that guarantees an optimal bistatic geometry (target far away from the baseline between the CPE and the SR). The numerical results shown in Fig. 14 can be obtained off-line, selecting for each point of the surveillance area the CPE that gives the minimum sum of the CRBs of the range and the bistatic velocity, i.e. the minimum trace of the sub-matrix $\mathbf{R}_k^{(m)}$ defined in Appendix B. Similarly, for each point of the surveillance area, the SR ranks the CPEs from the best to worst. This information represents the a priori knowledge about the scenario or the *memory* of the cognitive symbiotic radar.

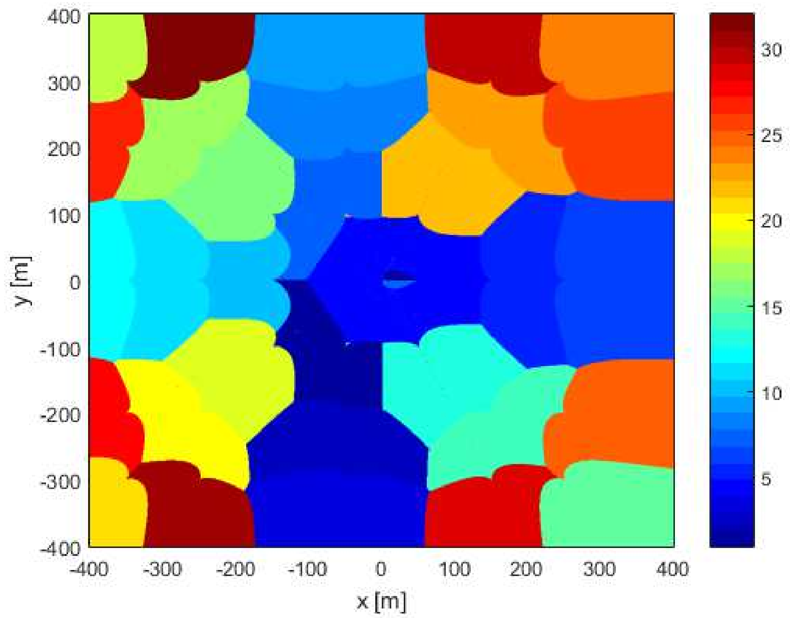

Fig. 14 – Map of the best CPE for each point of the surveillance area.

The perception-action cycle is based on the minimization of a pre-defined cost function. In 15 it is demonstrated that the cost function that minimizes the mean square error (MSE) of target state prediction is the trace of the prediction of the target state covariance matrix $\mathbf{P}_{k+1|k}$. This function is minimized when the transmitters of opportunity are the BS and all the M scheduled CPEs are those that minimize the measurement error, i.e. the CPEs for which the prediction point $\hat{\mathbf{x}}_{k+1|k}$ gives the lowest CRBs of the range and bistatic velocity.

Denoting by S_{ideal} this ideal set of M+1 (BS and the M CPEs) transmitters of opportunity, the minimum value of the cost function is given by $Trace\{\mathbf{P}_{k+1|k}(S_{ideal})\}$. Clearly, not all the available M slots in the US frame can be allocated for target tracking purposes, since the communication functionalities of the network must be preserved.

Let us denote by S_n the set of M+1 transmitters composed by the BS, the n CPEs (selected by the SR) that give the best performance in estimating the range and bistatic velocity, and the M-n CPEs selected by the BS for communication purposes. The cognitive passive tracking algorithm selects the set of transmitters for the subsequent frame by finding the minimum number n that guarantees a cost function such that

$$\lambda \cdot Trace\left\{\mathbf{P}_{k+1|k}\left(S_n\right)\right\} \leq Trace\left\{\mathbf{P}_{k+1|k}\left(S_{ideal}\right)\right\}, \tag{49}$$

where $0 \leq \lambda < 1$. The proposed idea described in (13) consists of selecting only a subset of the ideal transmitters of opportunity, allowing the BS to select the other

CPEs for communication purposes following its own priority rules. The threshold λ is used to select how the desired performance compares with of the ideal case.

Note that when λ=0, the tracking is purely passive and the SR does not select any CPE. In this case the SR will not improve the target tracking performance. On the other hand, when λ tends to 1, the SR improves tracking performance as closely to the ideal case as possible.

The search for the minimum number n of CPEs starts at 1, i.e. by exploiting the CPE that gives minimum error in estimating range and bistatic velocity, and it stops when $n=N_{MAX}$, i.e. when the maximum number of transmitter that can be scheduled for target tracking reaches that maximum value. The proposed algorithm is depicted in Table 2.

Among the M CPEs scheduled to transmit in each frame, the SR requests to the BS n (up to N_{MAX}) selected CPEs that improve radar performance. The remaining M-n bursts are allocated by the BS with its own rules to the other CPEs that request to transmit. Note that in the defined ComRadE system, the communication network cooperates with the SR, hence the CPEs, when selected by the SR, continue transmitting their own communication signal if they are asking to transmit, or emit a pseudo-random code in the other case. In any case, the scheduled CPEs do not transmit radar signals but IEEE 802.22 signals according to the standard. For this reason, if a CPE among those scheduled by the SR is a CPE which is asking to transmit, the communications functionality of the ComRadE system is preserved. On the other hand, a communication slot is lost if the CPE scheduled by the SR has not any communication signal to transmit and occupies the burst in the US with a pseudo-random signal.

The value of N_{MAX} can be tuned depending on how the ComRadE system gives priorities to the communication and the radar functionalities of the complete system. If N_{MAX} is fixed to zero, the ComRadE system is focused on the communication functionality only. On the other hand, if N_{MAX} is fixed to M, all the CPEs are scheduled by the SR and hence the ComRadE system focuses on the radar functionality. As will be clear in the next section, the value of n reaches N_{MAX} only for some unfavorable geometries and for values of λ that tend to 1. In practice, the number n of selected CPEs by the SR is often lower than the maximum number of CPEs that can be selected.

In this work and without loss of generality, we assume that N_{MAX}=$M/2$, i.e. when 50% of the available slots in the US can be allocated by the SR and the remaining by the BS.

According to the US time/frequency map (US-Map) depicted in Fig. 12, the algorithm also minimizes the resources allocated for target tracking, i.e. the minimum number n that allocates the CPEs for target tracking in the bursts with lower sub-channels per OFDM symbols is found. The remaining M-n bursts are allocated by the BS for communication purposes. Clearly, if these CPEs are in favorable bistatic geometries, they are also exploited for target tracking. It is also important to highlight that the n scheduled CPEs for target tracking purposes do not transmit specific radar signals, they instead, transmit their own communication data stream. The SR processes only the physical signal without extracting the information contained in the data stream.

In other words, the communication signal is also exploited for radar purposes and hence the n bursts are not exclusively used for target tracking. Hence, even in the case in which N_{MAX}=M and all the CPEs are scheduled by the SR, the communication functionality is not lost since the CPEs transmit their data stream. In this particular case, the BS losses its role for selecting the CPEs. In some practical examples, this can be also an advantage. Consider for example, the particular case in which all the CPEs are wireless cameras used for surveillance purposes. If the SR detects a target and has the highest priority in selecting the CPEs (N_{MAX}=M), along the target trajectory, the CPEs that are scheduled to transmit are those closer to the target (this will be clearer in the next section). In this case the SR achieves its best performance for target tracking and the data streams that can be processed at the BS are the videos recorded by the wireless cameras which are closer to the tracked target.

Table 2 – Algorithm used by the SR to select the best set of CPEs.

```
for each time instant k
    evaluate the ideal set S_ideal
    evaluate P_{k+1|k}(S_ideal)
    n=0
    while
λ·Trace{P_{k+1|k}(S_n)} > Trace{P_{k+1|k}(S_ideal)}
        n=n+1
        if n>N_MAX
            return
        else
            evaluate S_n
            evaluate P_{k+1|k}(S_n)
        end
    end
end
```

4. Simulation results

This section analyzes the performance of the proposed cognitive passive tracking algorithm for two simulated scenarios. The first scenario in the one shown in Fig. 13, where there are 32 CPEs, and the second scenario consists of the same surveillance area but considers an IEEE 802.22 WRAN with 256 CPEs. As shown in Fig. 13, the SR is located at the origin of the Cartesian coordinate system while, in absence of process noise, the target is moving from [-400 m, 400 m] to [400 m, -250 m], with speed 8.33 m/sec.

In the simulation runs, the process noise power q has been fixed to q=0.01, with this value the resulting trajectories in the Monte Carlo runs result close to the worst case trajectory depicted in Fig. 13 where the target approaches the SR introducing a strong non-linearity in the resulting bistatic geometry. Among the available CPEs in the network, only M=8 can be scheduled to transmit in each superframe. To improve target tracking performance and according to the proposed algorithm, the SR can select up to $M/2$=4 collaborative CPEs.

Figs. 4 and 5 show the Root Mean Square Error (RMSE) of the target position and velocity for the first scenario depicted in Fig. 13. The RMSEs are measured as follows

$$RMSE_{position} = \sqrt{\frac{1}{MC}\sum_{mc=1}^{MC}\left(x^{(mc)} - \hat{x}_{k|k}^{(mc)}\right)^2 + \left(y^{(mc)} - \hat{y}_{k|k}^{(mc)}\right)^2}\,, \quad (50)$$

$$RMSE_{velocity} = \sqrt{\frac{1}{MC}\sum_{mc=1}^{MC}\left(\dot{x}^{(mc)} - \hat{\dot{x}}_{k|k}^{(mc)}\right)^2 + \left(\dot{y}^{(mc)} - \hat{\dot{y}}_{k|k}^{(mc)}\right)^2} \quad (51)$$

The results have been obtained through MC=10^4 Monte Carlo runs for values of λ={0, 0.8, 0.9, 0.95, 0.99, 0.999}. The results obtained with λ=0 show the performance of a passive radar that does not exploit the cognitive perception-action cycle described in the previous section. That is when the SR does not select any CPE and the ComRadE system focuses only on the communication functionality.

For comparison purposes, the figures also show the RMSE for the ideal set of transmitters S_{ideal}, that is when all the M scheduled CPEs are those that provide the lowest measurement errors.

The degradation in performance for $k\in$ [400, 500] is related to the fact that in this time interval, the target approaches the SR. For the resulting geometry, the non-linearity in (5) is severe and the non-Gaussianity of the true posterior density is stronger 17. This phenomenon is more pronounced for low values of λ.

From these numerical results, it is apparent that there is a gain obtained using the cognitive tracking algorithm with respect to the purely passive tracking.

As discussed in the previous section, the proposed algorithm has been designed also to preserve the communication capabilities of the network. Fig. 17 shows the mean number of CPEs scheduled to transmit by the SR along the target trajectory, while Fig. 18 shows the percentage of resources occupied by these devices. The percentage of resources is the number of OFDM symbols and frequency sub-channel allocated by the SR over the total 15×60=900 time/frequency slots in the US-Map. In the particular case of this first result, Fig. 17 and Fig. 18 appear to achieve similar performances. This means that the n scheduled CPEs are mapped in the same burst of the US-Map to minimize the cost function. This results is related to the fact that in this scenario there are few CPEs. If the number of CPEs is increase, the difference between these two plots is more evident.

Clearly, when λ=0 the tracking is passive and the SR does not schedule any CPE while when λ approaches 1, the SR tends to schedule all the available $M/2$ CPEs. Note also that for the particular case of λ=0.95, the mean number of scheduled CPEs is not greater than 2, the percentage of resources allocated by the SR is not greater than 16%, and the resulting performances are substantially improved compared to the case of λ=0.

Note also that in the first analyzed scenario with only 32 CPEs, the performance in the case λ=0 is comparable with the other ones since there is a high probability that the 8 CPEs scheduled to transmit have favorable bistatic geometries. The performance of the cognitive algorithm is more prominent when the IEEE 802.22 WRAN is composed of a large number of CPEs.

Fig. 19 shows the best CPE for each point of the surveillance area when there are 256 CPEs, whose positions have been uniformly distributed in the 400 m × 400 m area. Figs. 9 and 10 show the resulting RMSE of position and velocity for the same target trajectory as that of Fig. 13, while Figs 11 and 12 show the number of CPEs scheduled by the SR and the corresponding allocated resources. The results have been obtained for the case of λ=0 and λ=0.95.

It is apparent in this case that the performance of the cognitive algorithm reaches that of the ideal case and the RMSE is lower than that of the purely passive system. Note also that in this particular case, the resources allocated by the SR are higher than in the case of 32 CPEs. This is due to the fact that with 256 available CPEs, the ideal cost function $Trace\{\mathbf{P}_{k+1|k}(S_{ideal})\}$ is lower than in the previous case and the cognitive algorithm needs more resources to satisfies (13).

Note also that in some points, such as for $k \in [100, 350]$, the behavior of the allocated resources in Fig. 23 is similar to the mean number of allocated transmitters in Fig. 22 but it is not a scaled version such as in the case of the scenario with 32 CPEs. This means that for some points along the target trajectory, even if the number n of allocated CPEs is the same, they are mapped in different data burst of the US-Map with the aim to minimize the percentage of allocated resources.

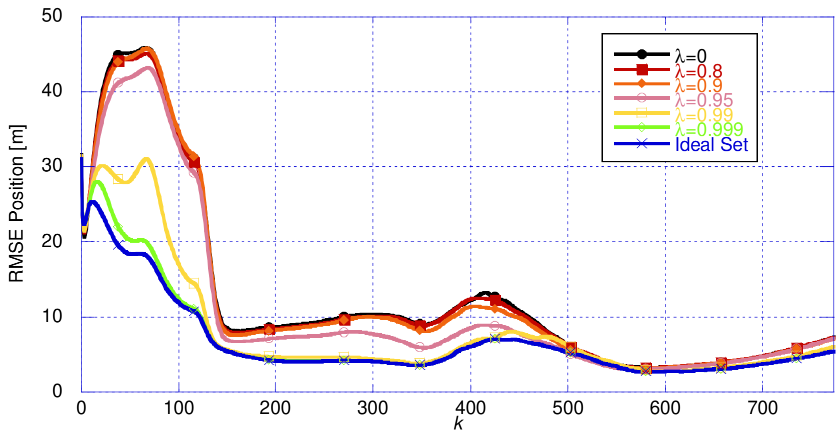

Fig. 15 – RMSE of target position for λ={0, 0.8, 0.9, 0.95, 0.99, 0.999}.

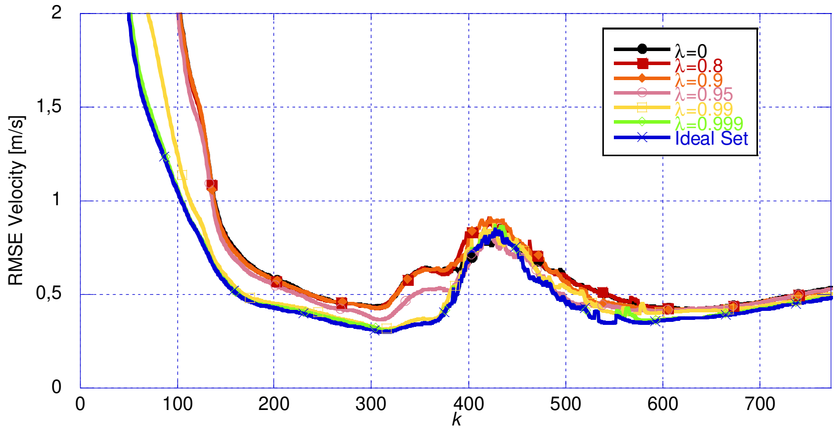

Fig. 16 - RMSE of target velocity for λ={0, 0.8, 0.9, 0.95, 0.99, 0.999}.

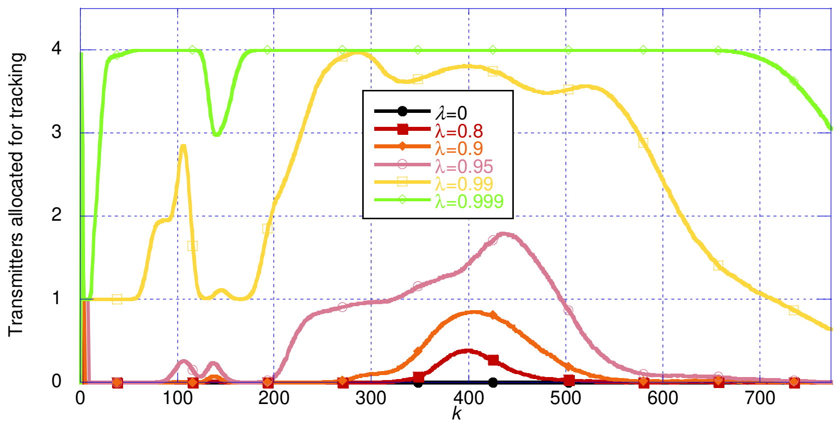

Fig. 17 - Mean number of CPEs scheduled to transmit by the SR.

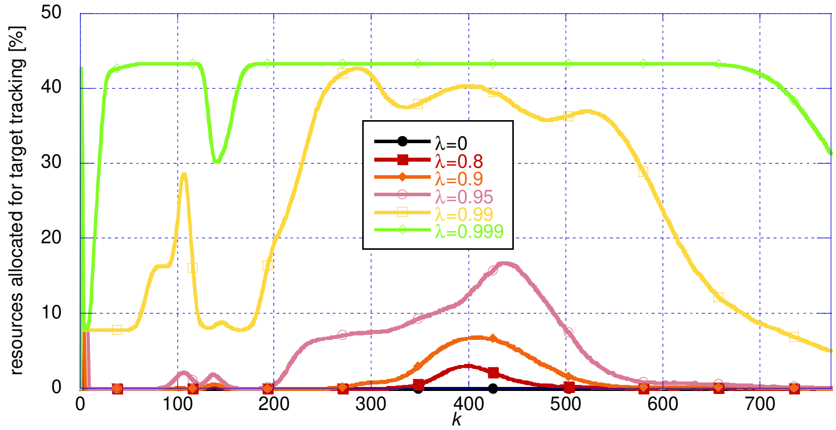

Fig. 18 – Percentage of resources allocated for target tracking.

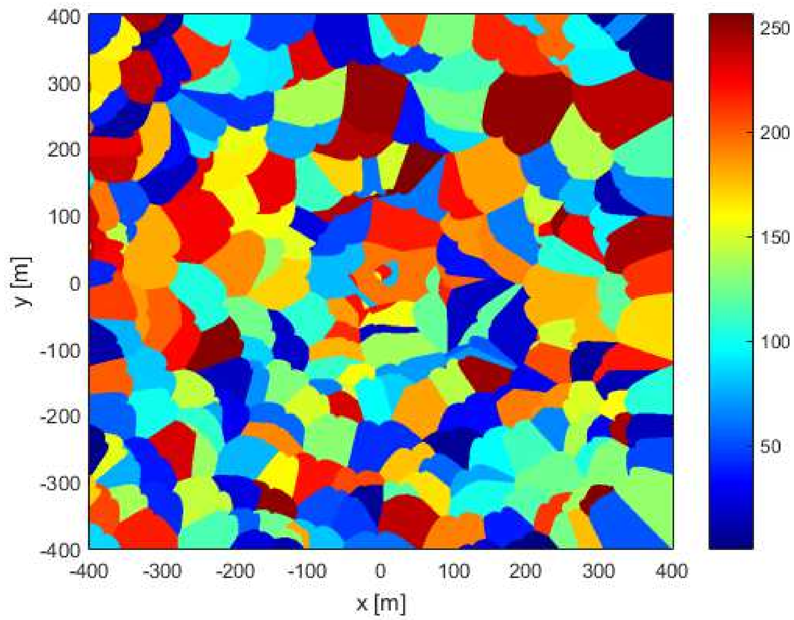

Fig. 19 – Map of the best CPE for each point of the surveillance area, 256 CPEs.

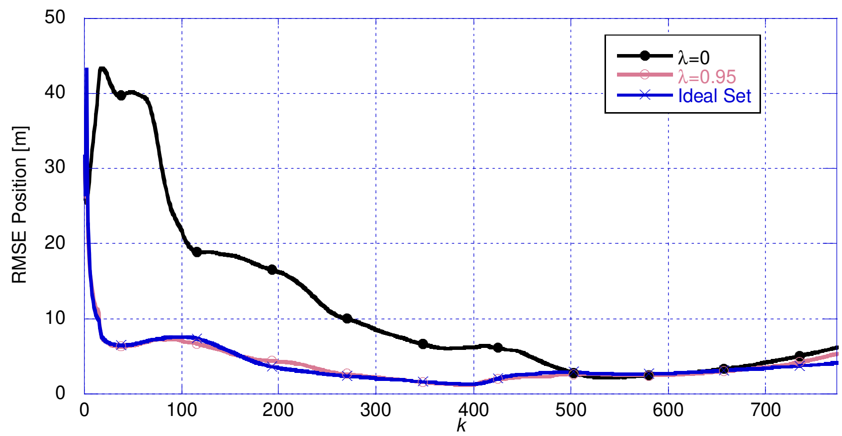

Fig. 20 - RMSE of target position for λ={0, 0.95}.

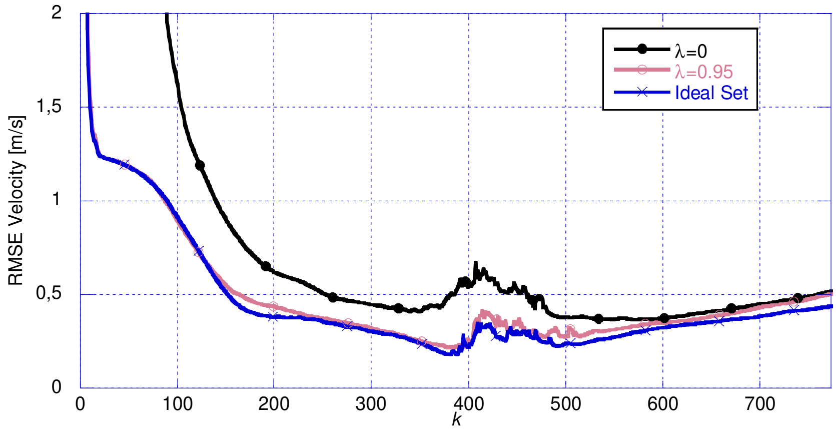

Fig. 21 - RMSE of target velocity for λ={0, 0.95}.

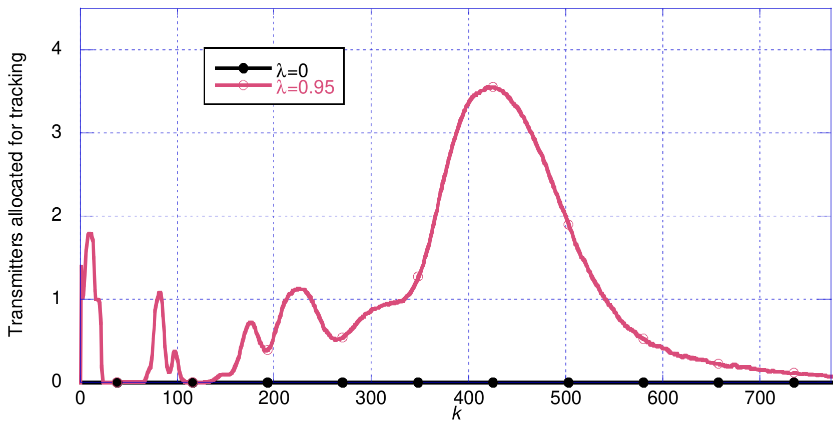

Fig. 22 - Mean number of CPEs scheduled to transmit by the SR.

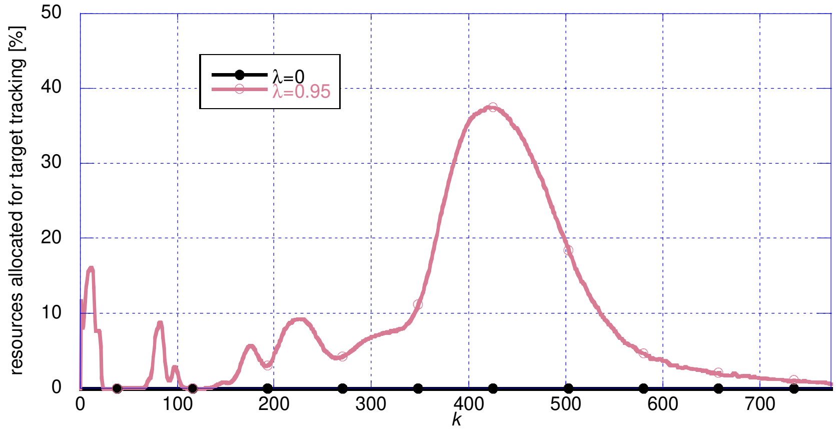

Fig. 23 - Percentage of resources allocated for target tracking.

5. Conclusions

In this work, we focus on a Symbiotic Radar, which is a passive radar fully integrated into a communication network. The resulting system is defined as a ComRadE system, where the communication and radar functionalities are jointly performed and the communication network and the passive radar are "friendly" or "allies". We focused on the particular case of an IEEE 802.22 WRAN. This choice has been made considering that both the SR, which is a passive system, and the IEEE 802.22 devices that exploit cognitive radio techniques, can be installed everywhere without any license to transmit and without interfere with other radiating systems. In this way, the occupied spectrum is used very efficiently for both radar and communication functionalities that can be operated simultaneously, which then guarantees a permanent availability of both functions and helps to overcome the limited availability of spectral resources for operations in spectrally crowded environments.

The symbiotic radar is integrated with the WRAN and can control the BS to select some of the CPEs scheduled to transmit. Recent research has been devoted to design and develop of such as system 7, to this end we defined a cognitive passive tracking algorithm inspired by the perception-action cycle introduced by Haykin 15, where the CPEs in each frame are selected to improve target tracking performance. The proposed algorithm is also designed to preserve the communication capabilities of the network. The obtained results show that there is a substantial gain using the proposed algorithm with respect to a passive radar that does not select the CPEs of opportunity even in the case in which the resources allocated to the SR are very low. Future research should also focus on a network of cooperative SRs equipped with IEEE 802.22 devices to share their detection and tracking information with a fusion center.

Appendix A – *Dependence of the measurement vector on the target state*.

The available measurements at time k are collected in a column vector $\mathbf{z}_k=[r_k^{(0)}\ \zeta_k^{(0)}\ \ldots\ r_k^{(M)}\ \zeta_k^{(M)}\ \theta_k]^T$, whose components are the range from receiver to target and the bistatic velocity, and the target DOA. The explicit expressions of the elements of $\mathbf{h}_k(\mathbf{x}_k)$ of (5) are 21:

$$r_k^{(m)} = \sqrt{x_k^2 + y_k^2}\ , \tag{52}$$

$$\zeta_k^{(m)} = \frac{\tilde{x}_k^{(m)}\dot{x}_k + \tilde{y}_k^{(m)}\dot{y}_k}{d_k^{(m)}}, \tag{53}$$

$$\theta_k = tg^{-1}\left(\frac{y_k}{x_k}\right), \tag{54}$$

for m=0,1,…,M and where ($\tilde{x}_k^{(m)}, \tilde{y}_k^{(m)}$) is the incenter at the target position of the m^{th} bistatic triangle and

$$d_k^{(m)} = \sqrt{\left(\tilde{x}_k^{(m)}\right)^2 + \left(\tilde{y}_k^{(m)}\right)^2}\ . \tag{55}$$

Recalling that the SR is at the origin of the Cartesian coordinate system and indicating with $l_k^{(m)}$ and $t_k^{(m)}$ the baseline between the m^{th} transmitter and the SR and the distance between the target and the m^{th} transmitter, respectively, the incenter at the target position is given by

$$\left(\tilde{x}_k^{(m)}, \tilde{y}_k^{(m)}\right) = \frac{l_k^{(m)}\left(x_k, y_k\right) + r_k^{(m)}\left(x_T^{(m)}, y_T^{(m)}\right)}{l_k^{(m)} + r_k^{(m)} + t_k^{(m)}} - \left(x_k, y_k\right), \tag{56}$$

where

$$l_k^{(m)} = \sqrt{\left(x_T^{(m)}\right)^2 + \left(y_T^{(m)}\right)^2}\ , \tag{57}$$

$$t_k^{(m)} = \sqrt{\left(x_k - x_T^{(m)}\right)^2 + \left(y_k - y_T^{(m)}\right)^2}\ . \tag{58}$$

The EKF exploits the Jacobian of $\mathbf{h}_k(\mathbf{x}_k)$ evaluated at $\hat{\mathbf{x}}_{k|k-1}$, and the explicit expression of the Jacobian matrix is given by 21:

$$\left[\nabla_{\mathbf{x}_k}\mathbf{h}_k^T(\mathbf{x}_k)\right]^T = \begin{bmatrix} \frac{\partial r_k^{(0)}}{\partial x_k} & \frac{\partial r_k^{(0)}}{\partial \dot{x}_k} & \frac{\partial r_k^{(0)}}{\partial y_k} & \frac{\partial r_k^{(0)}}{\partial \dot{y}_k} \\ \frac{\partial \zeta_k^{(0)}}{\partial x_k} & \frac{\partial \zeta_k^{(0)}}{\partial \dot{x}_k} & \frac{\partial \zeta_k^{(0)}}{\partial y_k} & \frac{\partial \zeta_k^{(0)}}{\partial \dot{y}_k} \\ \vdots & \vdots & \vdots & \vdots \\ \frac{\partial r_k^{(M)}}{\partial x_k} & \frac{\partial r_k^{(M)}}{\partial \dot{x}_k} & \frac{\partial r_k^{(M)}}{\partial y_k} & \frac{\partial r_k^{(M)}}{\partial \dot{y}_k} \\ \frac{\partial \zeta_k^{(M)}}{\partial x_k} & \frac{\partial \zeta_k^{(M)}}{\partial \dot{x}_k} & \frac{\partial \zeta_k^{(M)}}{\partial y_k} & \frac{\partial \zeta_k^{(M)}}{\partial \dot{y}_k} \\ \frac{\partial \theta_k}{\partial x_k} & \frac{\partial \theta_k}{\partial \dot{x}_k} & \frac{\partial \theta_k}{\partial y_k} & \frac{\partial \theta_k}{\partial \dot{y}_k} \end{bmatrix}, \tag{59}$$

where

$$\frac{\partial r_k^{(m)}}{\partial x_k} = \frac{x_k}{r_k^{(m)}}, \quad \frac{\partial r_k^{(m)}}{\partial y_k} = \frac{y_k}{r_k^{(m)}}, \tag{60}$$

$$\frac{\partial \zeta_k^{(m)}}{\partial x_k} = \frac{1}{\left(d_k^{(m)}\right)^2}\left[\left(\dot{x}_k \frac{\partial \tilde{x}_k^{(m)}}{\partial x_k} + \dot{y}_k \frac{\partial \tilde{y}_k^{(m)}}{\partial x_k}\right) d_k^{(m)} - \left(\tilde{x}_k^{(m)}\dot{x}_k + \tilde{y}_k^{(m)}\dot{y}_k\right)\frac{\partial d_k^{(m)}}{\partial x_k}\right], \tag{61}$$

$$\frac{\partial \zeta_k^{(m)}}{\partial y_k} = \frac{1}{\left(d_k^{(m)}\right)^2}\left[\left(\dot{x}_k \frac{\partial \tilde{x}_k^{(m)}}{\partial y_k} + \dot{y}_k \frac{\partial \tilde{y}_k^{(m)}}{\partial y_k}\right) d_k^{(m)} - \left(\tilde{x}_k^{(m)}\dot{x}_k + \tilde{y}_k^{(m)}\dot{y}_k\right)\frac{\partial d_k^{(m)}}{\partial y_k}\right], \tag{62}$$

$$\frac{\partial \zeta_k^{(m)}}{\partial \dot{x}_k} = \frac{\tilde{x}_k^{(m)}}{d_k^{(m)}}, \quad \frac{\partial \zeta_k^{(m)}}{\partial \dot{y}_k} = \frac{\tilde{y}_k^{(m)}}{d_k^{(m)}}, \tag{63}$$

$$\frac{\partial \theta_k}{\partial x_k} = -\frac{y_k}{\left(r_k^{(m)}\right)^2}, \quad \frac{\partial \theta_k}{\partial y_k} = \frac{x_k}{\left(r_k^{(m)}\right)^2}, \tag{64}$$

$$\frac{\partial r_k^{(m)}}{\partial \dot{x}_k} = \frac{\partial r_k^{(m)}}{\partial \dot{y}_k} = \frac{\partial \theta_k}{\partial \dot{x}_k} = \frac{\partial \theta_k}{\partial \dot{y}_k} = 0. \tag{65}$$

The derivatives that appear in (25) and (26) can be calculated straightforwardly.

Appendix B – *Covariance matrix of the measurement error*.

The measurement errors of the ranges and bistatic velocities from the M+1 transmitters of opportunity are independent as well as the measurement error of the DOA that depends on the half-power beamwidth of the receiver antenna. The resulting covariance matrix of the measurement vector is a block diagonal matrix given by

$$\mathbf{R}_k = diag\left(\mathbf{R}_k^{(0)},\ldots,\mathbf{R}_k^{(M)},\sigma_\theta^2\right) \tag{66}$$

where σ_θ^2 is the half-power beamwidth of the receiving antenna that in this work has been fixed to 3°, while $\mathbf{R}_k^{(m)}$ is the covariance matrix of the errors in measuring $r_k^{(m)}$ and $\zeta_k^{(m)}$. This matrix, which depends on the transmitted signal and on the m^{th} bistatic geometry, is given by 13

$$\mathbf{R}_k^{(m)} = \left[\mathbf{C}_k^{(m)}\left(\mathbf{E}_k^{(m)}\right)^{-1}\left(\mathbf{C}_k^{(m)}\right)^T\right]^{-1}, \tag{67}$$

where

$$\mathbf{E}_k^{(m)} = \frac{1}{2SNR_k^{(m)}}\begin{bmatrix}\left(\Delta\tau_k^{(m)}\right)^2 & 0\\ 0 & \left(\Delta\nu_k^{(m)}\right)^2\end{bmatrix}, \tag{68}$$

$$\Delta\tau_k^{(m)} = \frac{1}{|\Omega_m|\Delta f}, \quad \Delta\nu_k^{(m)} = \frac{1}{16T}, \tag{69}$$

directly depends on the delay and Doppler resolutions of the target echo from the signal emitted by the m^{th} transmitter, and the corresponding signal to noise ratio (SNR) at the radar receiver. On the other hand, the matrix $\mathbf{C}_k^{(m)}$ is given by 13, 21:

$$\mathbf{C}_k^{(m)} = \begin{bmatrix} \dfrac{\partial \tau_k^{(m)}}{\partial r_k^{(m)}} & \dfrac{\partial v_k^{(m)}}{\partial r_k^{(m)}} \\ \dfrac{\partial \tau_k^{(m)}}{\partial \zeta_k^{(m)}} & \dfrac{\partial v_k^{(m)}}{\partial \zeta_k^{(m)}} \end{bmatrix}, \tag{70}$$

and takes into account the effects of the bistatic geometry. This matrix is strictly related to the non-linear relations between the delay and the range and the Doppler shift and the bistatic velocity 13, 21:

$$\tau_k^{(m)} = \frac{r_k^{(m)} + \sqrt{\left(r_k^{(m)}\right)^2 + \left(l_k^{(m)}\right)^2 + 2 r_k^{(m)} l_k^{(m)} \sin \varphi_k^{(m)}}}{c}, \tag{71}$$

$$v_k^{(m)} = 2 \frac{f_0}{c} \zeta_k^{(m)} \sqrt{\frac{1}{2} + \frac{r_k^{(m)} + l_k^{(m)} \sin \varphi_k^{(m)}}{2\sqrt{\left(r_k^{(m)}\right)^2 + \left(l_k^{(m)}\right)^2 + 2 r_k^{(m)} l_k^{(m)} \sin \varphi_k^{(m)}}}}, \tag{72}$$

where f_0=600 MHz is the carrier frequency, c is the speed of light, while $\varphi_k^{(m)}$ is the receiver look angle and is given by 22

$$\varphi_k^{(m)} = \cos^{-1}\left(\frac{\left(r_k^{(m)}\right)^2 + \left(l_k^{(m)}\right)^2 - \left(t_k^{(m)}\right)^2}{2 r_k^{(m)} l_k^{(m)}} \right) - \frac{\pi}{2}. \tag{73}$$

Let

$$\omega_k^{(m)} = \left(r_k^{(m)}\right)^2 + \left(l_k^{(m)}\right)^2 + 2 r_k^{(m)} l_k^{(m)} \sin \varphi_k^{(m)}, \tag{74}$$

$$\bar{\omega}_k^{(m)} = r_k^{(m)} + l_k^{(m)} \sin \varphi_k^{(m)}, \tag{75}$$

$$\mu_k^{(m)} = 1 + \bar{\omega}_k^{(m)} \Big/ \sqrt{\omega_k^{(m)}}, \tag{76}$$

the elements of $\mathbf{C}_k^{(m)}$ are given by 13, 19, 21:

$$\frac{\partial \tau_k^{(m)}}{\partial r_k^{(m)}} = \frac{\mu_k^{(m)}}{c}, \quad \frac{\partial v_k^{(m)}}{\partial r_k^{(m)}} = \frac{\sqrt{2} f_C}{2c} \zeta_k^{(m)} \frac{\left(l_k^{(m)}\right)^2 \cos^2 \varphi_k^{(m)}}{\left(\omega_k^{(m)}\right)^{3/2} \left(\mu_k^{(m)}\right)^{1/2}}, \tag{77}$$

$$\frac{\partial \tau_k^{(m)}}{\partial \zeta_k^{(m)}} = 0, \quad \frac{\partial \nu_k^{(m)}}{\partial \zeta_k^{(m)}} = \frac{\sqrt{2} f_C}{c} \left(\mu_k^{(m)} \right)^{1/2}. \tag{78}$$

REFERENCES

1 Wicks, M., “Spectrum crowding and Cognitive Radar”, Cognitive Information Processing, 2010 International Workshop on, June 2010.

2 Stinco, P., Greco, M.S., Gini, F.; “Spectrum sensing and sharing for cognitive radars” (2016) IET Radar, Sonar and Navigation, 10 (3), pp. 595-602.

3 La Manna, M., Stinco, P., Greco, M., Gini, F., “Design of a cognitive radar for operation in spectrally dense environments”, (2013) IEEE National Radar Conference - Proceedings, art. no. 6585996, 29 April-3 May, 2013 Ottawa, Ontario, Canada.

4 Sturm, C.; Wiesbeck, W., “Waveform Design and Signal Processing Aspects for Fusion of Wireless Communications and Radar Sensing,” in Proceedings of the IEEE, vol.99, no.7, pp.1236-1259, July 2011.

5 Griffiths, H.; Darwazeh, I.; Inggs, M., “Waveform design for Commensal Radar,” in Radar Conference (RadarCon), 2015 IEEE , vol., no., pp.1456-1460, 10-15 May 2015

6 IEEE Std 802.22 “Part 22: Cognitive Wireless RAN Medium Access Control (MAC) and Physical Layer (PHY) Specifications: Policies and Procedures for Operation in the TV Bands”, 1 July 2011.

7 Wilson-Langman, A., Inggs, M.R., Mishra, A.K, Parent under review: "Symbiotic radar and communication system", Google Patents, WO Patent App. PCT/IB2014/059,036, 2014.

8 Mishra, A.K., Inggs, M., "White space symbiotic radar: a new scheme for coexistence of radio communication and radar" 2015 IEEE Radar Conference, Proceeding of, Johannesburg, South Africa, 27-30 October 2015.

9 Langman, A., Hazarika, O., Mishra, A.K., Inggs, M., "White RHINO: A low cost whitespace communications and radar hardware platform," Radioelektronika (RADIOELEKTRONIKA), 2013 23rd International Conference, Pardubice, 2013, pp. 240-244.

10 Hazarika, O., Mishra, A.K, "White RHINO—A New SDR Platform for Whitespace Communication", White Space Communication. Springer International Publishing, 2015. 195-219.

11 Mishra A.K.; Inggs M., “FOPEN capabilities of commensal radars based on whitespace communication systems,” Electronics, Computing and Communication Technologies (IEEE CONECCT), 2014 IEEE International Conference on, 6-7 Jan. 2014.

12 Stinco, P., Greco, M.S., Gini, F., “White space Passive Coherent Location system based on IEEE 802.22” (2015) Proceedings International Radar Symposium, art. no. 7226318, pp. 71-76, Germany, 24-26 June 2015.

13 Stinco, P., Greco, M., Gini, F., Himed, B., “Velocity profiler in IEEE 802.22 based PCL system” (2015) 2015 IEEE 6th International Workshop on Computational Advances in Multi-Sensor Adaptive Processing, CAMSAP 2015, art. no. 7383789, pp. 273-276, Cancun, Mexico , December 2015.

14 Brew M., Darbari F., Crockett L.H., Waddell M.B., Fitch M., Weiss S., Stewart R.W., “UHF white space network for rural smart grid communications”,

Smart Grid Communications (SmartGridComm), 2011 IEEE International Conference on, pp.138,142, 17-20 October 2011.

15 Haykin, S., “Cognitive Dynamic Systems: Perception-action Cycle, Radar and Radio”, Cambridge University Press, 2012.

16 Haykin, S., “Cognitive Radar: A way of the future”, IEEE Signal Processing Magazine, 23 (1), pp. 30-40, January 2006.

17 Ristic, B., Arulampalam, S., Gordon, N., “Beyond the Kalman Filter: Particle Filters for Tracking Applications”, Artech House, MA (2004).

18 Greco, M.S., Stinco, P., Gini, F., Farina, A., “Cramér-Rao bounds and selection of bistatic channels for multistatic radar systems”, (2011) IEEE Transactions on Aerospace and Electronic Systems, 47 (4), art. no. 6034675, pp. 2934-2948.

19 Stinco, P., Greco, M., Gini, F., Farina, A., “Cramér-Rao bounds and their application to sensor selection”, (2012) ICASSP, IEEE International Conference on Acoustics, Speech and Signal Processing - Proceedings, art. no. 6289091, pp. 5197-5200, Mar. 2012, Kyoto, Japan.

20 Rong Li, X., Jilkov, V.P., “Survey of Maneuvering Target Tracking. Part I: Dynamic Models”, IEEE Trans. on Aerospace and Electronic Systems, Vol. 39, No. 4, pp. 1333-1364, Oct. 2003.

21 Stinco, P., Greco, M.S., Gini, F., Farina, A., “Posterior Cramer-Rao Lower bounds for Passive bistatic radar tracking with uncertain target measurements” (2013) Signal Processing, 93 (12), pp. 3528-3540.

22 Jackson, M.C.; “The geometry of bistatic radar systems”, Communications, Radar and Signal Processing, IEE Proceedings F ,vol.133, no.7, pp.604-612, December 1986.

Publications under this Grant

[J1] P. Stinco, M. Greco, F. Gini, "Spectrum Sensing and Sharing for Cognitive Radars", IET Radar, Sonar and Navigation, Vol. 10, No 3, pp. 595–602, 2016

[J2] P. Stinco, M. Greco, F. Gini, B., Himed, "Cognitive Radars in Spectrally Dense Environments", IEEE AESS Magazine, Vol. 31, No. 10, pp. 20-27, October 2016, DOI: 10.1109/MAES.2016.150193.

[J3] P. Stinco, M. Greco, F. Gini, B. Himed, "IEEE 802.22 Passive Coherent Location: Multistatic Detection and Velocity Profiler", IEEE Transactions on Aerospace and Electronic Systems, Vol. 52, No. 5, pp. 2298-2312, October 2016.

[J4] P. Stinco, M. Greco, F. Gini, B. Himed, "Cognitive Passive Tracking in Symbiotic IEEE 802.22 ComRadE Systems", *IEEE Transactions on Aerospace and Electronic Systems*, April 2017.

[C1] P. Stinco, M. Greco, F. Gini, B. Himed, "Channel Parameters Estimation for Cognitive Radar Systems", *4th International Workshop on Cognitive Information Processing - CIP 2014*, May 26–28 2014, Copenhagen, Denmark.

[C2] P. Stinco, M. Greco, F. Gini, "White Space Passive Coherent Location System based on IEEE 802.22", *International Radar Symposium 2015* (IRS 2015), Dresden, Germany, 24-26 June 2015.

[C3] P. Stinco, M. Greco, F. Gini, B. Himed, "Velocity Profiler in IEEE 802.22 Based PCL System", *CAMSAP2015*, Cancun, Mexico, December 2015.

[C4] P. Stinco, M. Greco, F. Gini, B. Himed, "Cognitive Tracking in IEEE 802.22 Symbiotic Radars", *EUSIPCO 2016*, Budapest, August 2016.